New measures for characterizing nonlinear viscoelasticity in large amplitude oscillatory shear (LAOS)

Randy H. Ewoldt, A. E. Hosoi, and Gareth H. McKinley [a)]

Hatsopoulos Microfluids Laboratory, Massachusetts Institute of Technology,

Cambridge, MA 02139

Synopsis

Characterizing purely viscous or purely elastic rheological nonlinearities is straightforward using rheometric tests such as steady shear or step strains. However, a definitive framework does not exist to characterize materials which exhibit both viscous and elastic nonlinearities simultaneously. We define a robust and physically meaningful scheme to quantify such behavior, using an imposed large amplitude oscillatory shear (LAOS) strain. Our new framework includes new material measures and clearly defined terminology such as intra-/inter-cycle nonlinearities, strain-stiffening/softening, and shear-thinning/thickening. The method naturally lends a physical interpretation to the higher Fourier coefficients that are commonly reported to describe the nonlinear stress response. These nonlinear viscoelastic properties can be used to provide a "rheological fingerprint" in a Pipkin diagram that characterizes the material response as a function of both imposed frequency and strain amplitude. We illustrate our new framework by first examining prototypical nonlinear constitutive models (including purely elastic and purely viscous models, and the nonlinear viscoelastic constitutive equation proposed by Giesekus). In addition, we use this new framework to study

[a)] Author to whom correspondence should be addressed; electronic mail: gareth@mit.edu

experimentally two representative nonlinear soft materials, a biopolymer hydrogel and a wormlike micelle solution. These new material measures can be used to characterize the rheology of any complex fluid or soft solid and clearly reveal important nonlinear material properties which are typically obscured by conventional test protocols.

Keywords: Nonlinear viscoelasticity, Large amplitude oscillatory shear, LAOS, Chebyshev polynomial, FT rheology

I. INTRODUCTION

Biopolymer networks [Gardel *et al.* (2004), Storm *et al.* (2005), Chaudhuri *et al.* (2007)], wormlike micelles [Spenley *et al.* (1993)], colloidal gels [Gisler *et al.* (1999)], and metastable soft solids in general [Wyss *et al.* (2007)], exhibit complex nonlinear rheological responses, and as such have been of interest to experimentalists and theoreticians for many decades. The question arises of how to probe the complex viscoelastic response of such soft materials in the most appropriate way; see for example Philippoff (1966). Many of the biological and industrial processes associated with these materials cannot be described by steady shearing flow, nor by linear viscoelastic deformations constrained by small strain amplitudes. Large amplitude oscillatory shear (LAOS) [Dealy and Wissbrun (1990)] provides a method to quantify the progressive transition from linear to nonlinear rheological behavior as the strain amplitude γ_0 is increased at any given imposed frequency ω. The independent variables ω, γ_0 can be used to define the coordinate axes of a *Pipkin diagram* [Pipkin (1972)] which seamlessly connects steady viscometric flow (in the limit of small ω), linear viscoelasticity (in the limit of small γ_0), and nonlinear viscoelasticity. However, a comprehensive framework does not currently exist for quantifying in a physically meaningful way the nonlinear viscoelastic response that arises from this imposed deformation protocol. In this article, we develop a descriptive language and set of unambiguous material measures for quantifying the *nonlinear* viscoelastic response of soft materials, enabling us to develop a unique "rheological fingerprint" of an *a priori* unknown substance.

Both the elastic and viscous characteristics of an unknown material can be examined simultaneously by imposing an oscillatory shear strain, $\gamma(t) = \gamma_0 \sin(\omega t)$, which consequently imposes an orthogonal strain-rate $\dot{\gamma}(t) = \gamma_0 \omega \cos(\omega t)$. Here ω is the imposed oscillation

frequency, γ_0 is the strain amplitude, and t is time. At small strain amplitudes when the response is linear, the material is commonly characterized by the viscoelastic moduli $G'(\omega), G''(\omega)$, as determined from the components of the stress in phase with $\gamma(t)$ and $\dot{\gamma}(t)$ respectively [Ferry (1980)]. The strain amplitude γ_0 can be increased systematically to enter the nonlinear viscoelastic regime, resulting in a large amplitude oscillatory shear (LAOS) test. However, these linear viscoelastic moduli are not uniquely defined once the material response becomes nonlinear [Ganeriwala and Rotz (1987)], since a nonlinear stress response is not a single-harmonic sinusoid. Physical interpretation of the multitude of different material nonlinearities observed in LAOS tests is difficult, and widespread adoption of the technique has been hindered because an appropriate framework does not yet exist.

The most common method of quantifying LAOS tests is Fourier transform (FT) rheology [Wilhelm (2002)]. For a sinusoidal strain input $\gamma(t) = \gamma_0 \sin(\omega t)$, the stress response can be represented completely by a Fourier series [Dealy and Wissbrun (1990)], given in two alternate forms to emphasize either elastic or viscous scaling, respectively,

$$\begin{aligned} \sigma(t;\omega,\gamma_0) &= \gamma_0 \sum_{n\ \text{odd}} \left\{ G_n'(\omega,\gamma_0)\sin n\omega t + G_n''(\omega,\gamma_0)\cos n\omega t \right\} \\ \sigma(t;\omega,\gamma_0) &= \dot{\gamma}_0 \sum_{n\ \text{odd}} \left\{ \eta_n''(\omega,\gamma_0)\sin n\omega t + \eta_n'(\omega,\gamma_0)\cos n\omega t \right\}. \end{aligned} \quad (1)$$

Only odd-harmonics are included in this representation because the stress response is assumed to be of odd symmetry with respect to directionality of shear strain or shear-rate, i.e. the material response is unchanged if the coordinate system is reversed [Bird *et al.* (1987)]. Even-harmonic terms can be observed in transient responses, secondary flows [Atalik and Keunings (2004)], or dynamic wall slip [Graham (1995)], but these conditions will not be considered here. In the linear viscoelastic regime the stress response will include only the first harmonic, $n = 1$, whereas nonlinear material responses at larger strains result in the appearance and growth of higher harmonic contributions. Although

this FT framework is mathematically robust and reduces to the linear viscoelastic framework in the limit of small strains, it suffers from two drawbacks. First, although FT rheology is a very sensitive indicator of nonlinearity, as quantified by the Total Harmonic Distortion (T.H.D.) (e.g. Debbaut and Burhin (2002)) or the normalized intensity of the 3rd harmonic (e.g. Dotsch *et al.* (2003)), the FT framework does not result in a clear physical interpretation of the higher-order coefficients. Second, the use of the first-harmonic coefficients G_1' and G_1'' as measures of the viscoelastic moduli in the nonlinear regime (and which are often the output of commercial rheometers) is arbitrary and often fails to capture the rich nonlinearities that are apparent in the raw data signal.

A striking example of the shortcomings of the conventional FT rheology framework, and motivation for a new approach, is provided by the nonlinear viscoelastic response of native pedal mucus gel secreted by the terrestrial slug *Limax maximus* [Ewoldt *et al.* (2007)]. In the present work, a series of strain-controlled oscillatory tests at a fixed frequency of $\omega = 3\,\text{rad.s}^{-1}$ is imposed and the corresponding nonlinear behavior of the physically cross-linked mucus gel (see Section IV.A. Experimental methods) is shown in FIG. 1. The typical rheometric measures of viscoelastic moduli are shown in FIG. 1a and appear unremarkable. By contrast FIG. 1b shows the raw data measured by the torque transducer at each imposed frequency; the periodic stress response $\sigma(t;\omega,\gamma_0)$ at steady state is plotted parametrically against $\gamma(t)$. These parametric plots are commonly called Lissajous curves, or more accurately Lissajous-Bowditch curves,† and are frequently used to represent the raw material test data obtained from LAOS (e.g. Philippoff (1966)). A linear viscoelastic response appears as an ellipse, which contains two mirror planes (the major and minor axes of the ellipse). A steady nonlinear viscoelastic response loses the mirror planes and requires

† Orbital trajectories bearing J. A. Lissajous' name were studied by N. Bowditch in 1815, predating Lissajous' treatment in 1857 by more than forty years [Crowell (1981)]

only that the response is periodic, $\sigma(t) = \sigma(t+T)$ where T is the period of oscillation, allowing both odd and even harmonics in the Fourier series stress response. For the common situation of a simple fluid in which the material behaves the same in both shear directions, only odd harmonics are allowed (Eq. (1)) and the Lissajous-Bowditch curve maintains a rotational symmetry about the origin (rotation by π radians). We refer to the curves of $\sigma(t)$ vs. $\gamma(t)$ as *elastic* Lissajous-Bowditch curves to distinguish them from the *viscous* Lissajous-Bowditch curves which represent $\sigma(t)$ as a function of the imposed shear-rate $\dot{\gamma}(t)$.

The "elastic modulus" of pedal mucus reported by a rheometer (i.e. the first harmonic elastic modulus, G_1') decreases slightly with strain amplitude (FIG. 1a), implying minor strain-softening. However, the raw data in the form of Lissajous-Bowditch curves (FIG. 1b) reveal a strong nonlinear response evocative of strain-stiffening. The elastic Lissajous curves in FIG. 1b are elliptical for small γ_0 (see inset), but become progressively distorted in the nonlinear regime. At large strains, the shear stress is greater than one would expect by projecting the center portion of the ellipse, suggesting pronounced elastic strain-stiffening at large strain amplitudes which is not captured by the first harmonic elastic modulus.

This paradoxical behavior is not unique to pedal mucus but appears to be common in soft biological materials and can been seen, for example, in data reported by Ma *et al.* (1999) for a keratin filament network; in both cases strain-stiffening is suggested in the elastic Lissajous-Bowditch curves even though the familiar "viscoelastic moduli" do not appear to increase as a function of imposed strain amplitude γ_0. A quantitative measure for easily identifying and comparing this type of stiffening response does not currently exist.

In addition to FT rheology, various other methods have been proposed for quantifying nonlinear viscoelasticity in LAOS [Tee and Dealy (1975); Cho *et al.* (2005); Klein *et al.* (2007)].

However, these techniques either lack physical interpretation, cannot be calculated uniquely, or do not apply generally to all viscoelastic materials. Tee and Dealy (1975) offered three measures for quantifying viscous Lissajous-Bowditch curves of stress vs. strain-rate. Their material function which quantified a non-elliptical shape of a single curve was useful for indicating nonlinearity but offers no physical interpretation. A recently proposed decomposition into characteristic response functions [Klein *et al.* (2007), Klein *et al.* (2008)] uses sets of sine, square, and triangular waves to describe a prototypical nonlinear response. These selected waveforms may be thought of as a set of "basis functions" used to represent a superposition of different physical phenomena. Although this provides a very useful step toward a physical interpretation, these basis functions are not mutually orthogonal, in contrast to the harmonic series that form the basis of FT-rheology. They therefore blur measurement of the linear viscoelastic response and qualitative interpretations of the progressive onset of nonlinearity. Similarly, the so-called geometrical interpretation (also referred to as stress decomposition) introduced by Cho *et al.* (2005) suffers from non-orthogonality of the resulting material measures. For a single harmonic sinusoidal strain input, the geometrical interpretation decomposes the generic nonlinear stress response into a superposition of "elastic" and "viscous" contributions using symmetry arguments (further details are provided in Section II.a). Although this decomposition is unique, the resulting material parameters associated with the decomposition are not unique due to the non-orthogonality of the describing basis functions, as we outline below. It is therefore desirable to develop a complete, low-dimensional framework for quantifying nonlinear viscoelasticity which avoids these ambiguities.

We also note that alternate experimental protocols exist for measuring nonlinear oscillatory rheology which are not contained within the rubric of LAOS. The most common of these techniques is to measure a *differential modulus* [Janmey *et al.* (1983), Gardel *et al.* (2004), Yao *et al.* (2008)] from a small amplitude oscillatory shear deformation that is superposed upon a fixed bias

strain or stress. This protocol is quite useful for materials dominated by elasticity, but is less robust for materials which relax and flow under the constant imposed bias strain (or stress). Therefore, the differential modulus protocol cannot be applied readily to viscoelastic fluids in general.

In this manuscript we introduce a comprehensive framework for physically interpreting the deviations from a linear response to an imposed oscillatory shear deformation. This framework provides a geometric representation and a descriptive language for qualitatively familiar, but poorly defined, adjectives such as elastic stiffening/softening and viscous thickening/thinning. We use idealized models as well as experimental results to illustrate the use of these ideas. We also propose several new measures for reporting the first-order (linear) viscoelastic moduli in the nonlinear regime, to complement the first-order Fourier coefficients which are often insufficient to describe the material response. These additional measures all reduce to $G'(\omega)$ in the linear regime, but diverge systematically when applied to a nonlinear signal, offering additional physical insight into the underlying rheological response which would otherwise be obscured by conventional measures.

II. THEORY

A. Interpretation of higher harmonics

To interpret LAOS data in a physically meaningful way, we first extend the method of orthogonal stress decomposition [Cho *et al.* (2005)], which uses symmetry arguments to decompose the generic nonlinear stress response into a superposition of an elastic stress $\sigma'(x)$, where $x = \gamma / \gamma_0 = \sin \omega t$, and viscous stress $\sigma''(y)$ where $y = \dot{\gamma} / \dot{\gamma}_0 = \cos \omega t$. The total oscillatory stress is the sum of the two contributions, $\sigma(t) = \sigma'(t) + \sigma''(t)$. This decomposition is based on the idea that the elastic stress σ' should exhibit odd-symmetry with respect to x and even-symmetry with

respect to y, whereas viscous stress σ'' should exhibit even-symmetry with respect to x and odd-symmetry with respect to y. The decomposition is defined below [Cho *et al.* (2005)], and using this definition, along with Eq. (1) we indicate here that these elastic and viscous stresses are related directly to the Fourier decomposition as follows,

$$\begin{aligned}\sigma' &\equiv \frac{\sigma(\gamma,\dot{\gamma})-\sigma(-\gamma,\dot{\gamma})}{2} = \gamma_0 \sum_{n\ \text{odd}} G_n'(\omega,\gamma_0)\sin n\omega t \\ \sigma'' &\equiv \frac{\sigma(\gamma,\dot{\gamma})-\sigma(\gamma,-\dot{\gamma})}{2} = \gamma_0 \sum_{n\ \text{odd}} G_n''(\omega,\gamma_0)\cos n\omega t.\end{aligned} \tag{2}$$

Thus, in contrast to the closed loops formed by the total stress σ vs. γ or σ vs. $\dot{\gamma}$, plotting elastic stress σ' vs. x or viscous stress σ'' vs. y produces single-valued functions of strain or strain-rate respectively. FIG. 2 illustrates this stress decomposition using the LAOS experimental data for native pedal mucus shown in FIG. 1. The intra-cycle elastic and viscous nonlinearities (i.e. nonlinearities *within* a given steady state cycle at fixed ω,γ_0) are therefore related to the nonlinearity of these functional forms. Cho *et al.* (2005) suggest a polynomial regression fit to these lines of elastic and viscous stress (see their Eq. (23)). However, the material properties represented by the polynomial coefficients are not unique since they depend on the order of the polynomial arbitrarily chosen by the user. For example, given an unknown smooth function $F(x)$, a regression fit to a first order polynomial $F = a_0 + a_1 x$ will always result in different coefficients a_0, a_1 than a regression fit to the higher-order polynomial $F = a_0 + a_1 x + a_2 x^2 + \ldots$ except in the limit of $x \ll 1$ or if the unknown function is itself a linear function. Thus, fitting higher order terms affects the values of lower order terms, and polynomial regression fits do not result in unique values for quantifying nonlinearity. A framework which breaks down beyond the limit $x \ll 1$ is not suitable for quantifying a nonlinear (viscoelastic) response.

What is desired is an approach in which one fits $F = a_0 f_0(x) + a_1 f_1(x) + a_2 f_2(x) + \ldots$ such that incorporation of higher order terms does not affect lower order terms, i.e. the $f_i(x)$ must be orthogonal over the finite integration domain, in this case [-1,1]. These functions $f_i(x)$ are basis functions, and for the present case in which we decompose the stress into terms $\sigma'(x)$ and $\sigma''(y)$, where $x = \gamma/\gamma_0$ and $y = \dot{\gamma}/\dot{\gamma}_0$, the domain limits are the same for each curve, $-1 \le x, y \le 1$. Various sets of orthogonal polynomial basis functions exist, including Laguerre, Hermite, Jacobi, Utraspherical (Gegenbauer), Legendre, and Chebyshev of the first and second kind [Abramowitz and Stegun (1964)]. The appropriate set of polynomials for describing $\sigma'(x)$ and $\sigma''(y)$ will exhibit (i) orthogonality over a finite domain, (ii) odd symmetry about x=0 and (iii) a bounded range for higher-order contributions. By process of elimination, we argue that the logical choice for understanding LAOS is the set of Chebyshev polynomials of the first kind. Laguerre and Hermite polynomials are eliminated because their limits of orthogonality are [0,∞] and [-∞,∞], which contradicts the finite domain criteria. Jacobi polynomials are not appropriate, as they do not have symmetry about x=0 (except for special cases in which Jacobi polynomials can be related to Ultraspherical polynomials). Ultraspherical and Chebyshev (second kind) are ill-suited for LAOS due to their values at x=±1; higher harmonics have ever-larger maxima, or for some classes of Ultraspherical polynomials have ever-decreasing maxima. Finally, Legendre polynomials are eliminated because they are not directly related to the time-domain Fourier coefficients, thus implementation with previously reported LAOS data and comparison with other LAOS interpretations would be unnecessarily complicated. We therefore make the choice to select Chebyshev polynomials of the first kind, because these functions are bounded, exhibit symmetry about x=0, are orthogonal on the finite domain [-1,+1], and can easily be related to the Fourier

coefficients which have dominated the discussion on quantitative LAOS analysis. Using this basis set, the elastic and viscous contributions to the measured stress response can be written as

$$\begin{aligned}\sigma'(x) &= \gamma_0 \sum_{n:\text{ odd}} e_n(\omega,\gamma_0) T_n(x) \\ \sigma''(y) &= \dot{\gamma}_0 \sum_{n:\text{ odd}} v_n(\omega,\gamma_0) T_n(y)\end{aligned} \tag{3}$$

where $T_n(x)$ is the *n*th-order Chebyshev polynomial of the first kind, and $x = \gamma/\gamma_0$, $y = \dot{\gamma}/\dot{\gamma}_0$ provide the appropriate domains of [-1,+1] for orthogonality. The first, third, and fifth Chebyshev polynomials of the first kind are shown in the Appendix for reference, in addition to their equations and orthogonality relations. The functions at each order are orthonormal and therefore the coefficients e_n, v_n are independent of each other. We refer to $e_n(\omega,\gamma_0)$ as the elastic Chebyshev coefficients and $v_n(\omega,\gamma_0)$ as the viscous Chebyshev coefficients.

In the linear regime $e_3/e_1 \ll 1$ and $v_3/v_1 \ll 1$, and Eq. (3) recovers the linear viscoelastic result such that $e_1 \to G'$ and $v_1 \to \eta' = G''/\omega$. We interpret any deviation from linearity, i.e. the $n = 3$ harmonic, as follows. A positive contribution of the third-order polynomial $T_3(x) = 4x^3 - 3x$ results in a higher elastic stress at the maximum dimensionless strain, $x \to 1$ than is represented by the first-order contribution alone. Thus $e_3 > 0$ corresponds to intra-cycle strain-stiffening of the elastic stress, whereas $e_3 < 0$ indicates strain-softening. Similarly, a positive value for v_3 represents intra-cycle shear-thickening of the viscous stress, and $v_3 < 0$ describes shear-thinning. These physical interpretations are not apparent in the time-domain (Fourier coefficients) but become immediately apparent from the sign of the Chebyshev coefficients.

Our deliberate use of Chebyshev polynomials allows the coefficients e_n and v_n (Eq. (3)) to be calculated from the familiar Fourier coefficients (Eq. (1)). We use the identity

$T_n(\cos\theta)=\cos(n\theta)$, together with $\sin\theta=\cos(\pi/2-\theta)$ which gives $T_n(\sin\theta)=\sin(n\theta)(-1)^{\frac{n-1}{2}}$ for $n:\text{odd}$ (see Appendix for details). The relationships between the Chebyshev coefficients in the strain or strain-rate domain and the Fourier coefficients in the time domain are thus given by

$$\begin{aligned} e_n &= G_n'\left(-1\right)^{\frac{n-1}{2}} \quad n:\text{odd} \\ v_n &= \frac{G_n''}{\omega}=\eta_n{}' \quad n:\text{odd}\,. \end{aligned} \tag{4}$$

Thus, just as the third-order Chebyshev coefficients provide physical insight into the deviation from linear viscoelasticity, as described above, the third-order Fourier coefficients can also now be given a physical interpretation (with appropriate sign correction for G_3'). This new framework allows Fourier coefficients to be used to calculate physically meaningful measures of nonlinearity, i.e. the elastic and viscous Chebyshev coefficients.

Some researchers report results from FT rheology in terms of amplitude and phase, e.g. Reimers and Dealy (1996), in which Eq.(1) would take the form

$$\sigma=\gamma_0\sum_{n:\text{ odd}}\left|G_n^*\right|\sin\left(n\omega t+\delta_n\right) \tag{5}$$

where $\left|G_n^*\right|=\sqrt{G_n'+G_n''}$ is the scaled stress magnitude and δ_n is the phase with respect to the input strain signal $\gamma(t)=\gamma_0\sin\omega t$. The variable δ_n may be interpreted as determining the initial conditions of the higher-harmonic contributions. For example, at $\omega t=0$ the third harmonic contribution is $|G_3^*|\sin(\delta_3)$, and subsequently oscillates with a frequency of $3\omega_1$ for $\omega t>0$. Thus, δ_3 determines the initial value of the third-harmonic contribution, and must range from $0\le\delta_3\le 2\pi$.

As we noted above, only the signs of the third harmonic Chebyshev coefficients are needed to interpret the nature of elastic and viscous nonlinearities. Here they are related to the n=3 phase

angle and our interpretation of intra-cycle stiffening/softening and thickening/thinning can be summarized as

$$e_3 = -\left|G_3^*\right|\cos\delta_3 \begin{cases} >0 & \text{for } \pi/2 < \delta_3 < 3\pi/2 \quad \text{strain-stiffening} \\ =0 & \text{for } \delta_3 = \pi/2,\ 3\pi/2 \quad \text{linear elastic} \\ <0 & \text{for } -\pi/2 < \delta_3 < \pi/2 \quad \text{strain-softening} \end{cases}$$

$$v_3 = \frac{\left|G^*_3\right|}{\omega}\sin\delta_3 \begin{cases} >0 & \text{for } 0 < \delta_3 < \pi \quad \text{shear-thickening} \\ =0 & \text{for } \delta_3 = 0,\ \pi \quad \text{linear viscous} \\ <0 & \text{for } \pi < \delta_3 < 2\pi \quad \text{shear-thinning} \end{cases}$$

If only torque and displacement signals are available, rather than stress and strain, it is common to report the scaled intensity of the third harmonic torque response, I_3 / I_1, where I_n is the magnitude of the *n*-harmonic torque signal. One may calculate the scaled third harmonic Chebyshev coefficients as $e_3 / e_1 = (I_3 / I_1)\cos\delta_3 / \cos\delta_1$ and $v_3 / v_1 = (I_3 / I_1)\sin\delta_3 / \sin\delta_1$, the signs of which have an equivalent interpretation to e_3 and v_3, respectively, since e_1 and v_1 are always positive.

Other attempts have been made to physically interpret the phase of the 3rd harmonic, e.g. Neidhofer *et al.* (2003). Our interpretation is distinct in that the phase angle δ_3 indicates the nature of both the elastic *and* viscous nonlinearities, even when they occur simultaneously. Furthermore, in our framework this interpretation is based on the absolute phase difference relative to the excitation (δ_3). By contrast, in the work of Neidhofer *et al.* (2003) the relative phase with respect to the first harmonic ($\delta_3 - \delta_1$) is used. The above result suggests that the sign of both the elastic and viscous deviation from linearity is captured by a single quantity, δ_3. The interpretation of the higher harmonic stress response (G_3', G_3'', and the absolute phase δ_3) is thus facilitated by the use of our elastic and viscous Chebyshev coefficients e_3 and v_3.

B. Meaningful viscoelastic moduli in the nonlinear regime

The second issue we address with our new framework is the lack of clearly defined viscoelastic moduli for a nonlinear material response. The frequently used first-harmonic coefficients G_1' and G_1'' often fail to capture the rich nonlinearities that are apparent in the raw data signal (as shown in FIG. 1). We define here several new measures for accurately reporting the magnitudes of the first-order (linear) viscoelastic moduli in the nonlinear regime, each of which has a distinct physical interpretation and complements the often-reported first-order Fourier coefficients. These additional measures are deliberately chosen such that they reduce to the unique material functions $G'(\omega)$ or $G''(\omega)$ in the linear regime, but diverge systematically when used to analyze a nonlinear signal, offering additional physical insight beyond that captured by the average measures G_1', G_1''. The variation in these new measures can be reported as a function of imposed strain amplitude γ_0 (or strain-rate amplitude $\dot{\gamma}_0 = \gamma_0\omega$) to indicate the nature of material nonlinearity across different steady state cycles (i.e. inter-cycle nonlinearities).

1. Elastic modulus

We address the apparent contradiction of FIG. 1 by first recognizing that G_1' can be a misleading measure of the "elastic modulus" of such a material, since other harmonic components may also store energy [Ganeriwala and Rotz (1987)]. The first-harmonic represents a sine transform $G_1' = \omega/\left(\pi\gamma_0^{\,2}\right)\oint\sigma(t)\gamma(t)dt$, which is a measure of the average elasticity in the material response at each imposed pair of LAOS coordinates $\{\omega,\gamma_0\}$, and is therefore unable to distinctly represent the local elastic response of a material at small and large instantaneous strains. To capture this local behavior, we define a set of elastic moduli that are geometrically-motivated and then derive their relation to both conventional FT rheology descriptions (by substituting Eq. (1) into the definitions)

and our new Chebyshev stress decomposition (via Eq. (4)). We introduce the following definitions:

$$G'_M \equiv \left.\frac{d\sigma}{d\gamma}\right|_{\gamma=0} = \sum_{n \text{ odd}} nG'_n = e_1 - 3e_3 + \ldots \tag{6}$$

$$G'_L \equiv \left.\frac{\sigma}{\gamma}\right|_{\gamma=\gamma_0} = \sum_{n \text{ odd}} G'_n (-1)^{\frac{n-1}{2}} = e_1 + e_3 + \ldots \tag{7}$$

where G'_M is the *minimum-strain modulus* or tangent modulus at $\gamma = 0$ and G'_L is the *large-strain modulus* or secant modulus evaluated at the maximum imposed strain. The definitions of G'_M and G'_L can be considered as methods for calculating G' from available raw data, since for a linear viscoelastic response each is equivalent to G' (similarly, G'_1 is also equivalent to G' for a linear viscoelastic response). These measures can easily be visualized graphically using typical Lissajous-Bowditch curves as shown in FIG. 3a (linear response) and FIG. 3c (nonlinear response). These measures are deliberately chosen such that both converge to the linear elastic modulus $G'(\omega)$ in the limit of small strains ($e_3 / e_1 \ll 1$), i.e. $G'_L = G'_M = G'_1 = G'(\omega)$ in the linear regime, as seen from Eqs. (6)-(7). The corresponding Lissajous-Bowditch curve is an ellipse with local tangent at $\gamma = 0$ parallel to a secant at $\gamma / \gamma_0 = x = 1$. Although these new elastic measures are calculated from the total stress signal, they can also be related to the elastic stress σ' as decomposed by the geometrical interpretation of Cho *et al.* (2005). Thus, another useful measure of elasticity may be the slope of the elastic stress at maximum strain, $G'_K \equiv d\sigma' / d\gamma\big|_{\gamma=\gamma_0}$, which is reminiscent of a differential modulus for a given strain amplitude. We note that one might be tempted to take the local slope of the *total* stress near maximum strain as a type of elastic modulus, however this measure does not reduce to $G'(\omega)$ in the linear regime.

The minimum-strain modulus G'_M is the tangent modulus at zero instantaneous strain. This is a natural way to measure an elastic modulus. By the nature of an oscillatory test for which $\gamma(t) = \gamma_0 \sin(\omega t)$, at the point where $\gamma = 0$ the strain-rate is at a local maximum, $d\dot{\gamma}/dt = 0$ and the viscous contribution to the stress is thus locally constant. However, the strain *is* changing, which suggests that any change in stress should be related only to elasticity. In fact, this is a possible way to measure G' in the linear regime, since for small total deformations $G'_M \to G'$, but the formulation of Eq. (6) offers an interpretation of the elastic modulus in the nonlinear regime which is distinct from G'_1.

The large-strain modulus, G'_L, is the secant modulus at maximum strain. This is also a natural measurement of an elastic modulus since for $\gamma = \gamma_0$, we have $\dot{\gamma} = 0$, which suggests that the instantaneous viscous stress at this point should be zero. Accordingly, the total residual stress in the sample results only from the elastic characteristics of the soft material. The result is that $G'_L \to G'$ in the linear regime (small γ_0), but Eq. (7) offers an alternative and distinct view of the nonlinear elastic response.

The graphical representation of these measures aids our interpretation of Lissajous-Bowditch curves in both the linear and nonlinear regime. A Lissajous-Bowditch curve in the linear regime will appear as an ellipse. A common misconception is that the slope of the semi-major axis of this ellipse represents the elastic modulus (this slope actually represents the magnitude of the complex modulus). The elastic modulus is represented by the tangent slope at zero strain, G'_M, and the slope of the secant at maximum strain, G'_L. The secant at maximum strain is *not* equal to the semi-major axis of the ellipse, except for the case of a purely elastic solid whose Lissajous-Bowditch curve would appear as a straight line.

Using these graphical interpretations, it can be observed from the elastic Lissajous-Bowditch curves of FIG. 1b that for large imposed strain amplitude γ_0 the material is strain-stiffening within a given cycle (intra-cycle stiffening) since $G'_L > G'_M$. As the strain amplitude is varied, it is also observed that the tangent modulus G'_M decreases, indicating a type of inter-cycle softening of the elasticity at low strains. These insights can not be gained from reporting G'_1 alone.

We now have three ways to report the first-order elastic modulus: $G'_1 = e_1$, $G'_M = e_1 - 3e_3 + \ldots$, and $G'_L = e_1 + e_3 + \ldots$. These can be thought of as three different ways to approximate the leading order response of a nonlinear viscoelastic material. FIG. 4 depicts the use of these three elastic moduli in the approximation of an intra-cycle strain-stiffening nonlinear model. The simulated response is described by $G'_1 = 1\,\text{Pa}$, $e_3 = -G'_3 = 0.2\,\text{Pa}$, $v_1 = G''_1/\omega = 0.1$ Pa.s, and $v_3 = 0$, with all other higher harmonic contributions being identically zero. The minimum- and large-strain elastic moduli can be found from the model parameters by use of Eqs. (6)-(7). The linear approximation to the nonlinear viscoelastic response can be represented by using any of the first-order elastic moduli along with the loss modulus $\{G'_1, G''\}$, $\{G'_M, G''\}$, $\{G'_L, G''\}$ to create elliptical Lissajous-Bowditch curves. As can be seen in FIG. 4, the first-order Fourier elastic modulus G'_1 is a type of average elastic response. The small-strain modulus G'_M approximates the linear viscoelastic response as an ellipse that matches the small-strain elasticity. The linear approximation using the large-strain modulus G'_L captures the large-strain elasticity by matching the stress response at maximum strain.

2. Dynamic viscosity

It has been previously shown that under oscillatory shear deformation, all of the dissipated energy is represented by the first-harmonic loss modulus G''_1 [Ganeriwala and Rotz (1987),

Giacomin and Dealy (1993)]. The total energy dissipated per cycle per unit volume is $E_d = \pi\gamma_0^{\,2} G_1''$. While $G_1'' = \eta_1'\omega$ represents the total dissipation per cycle, it cannot differentiate between any local changes in the coefficient of viscous dissipation between the lowest and highest instantaneous shear-rates experienced during the oscillatory deformation. We therefore regard $G_1'' = \eta_1'\omega$ as representing an average dissipation coefficient over the cycle. Here we introduce new measures η_M' and η_L' which indicate the instantaneous viscosity (or coefficient of viscous dissipation) at the smallest and largest shear-rates, respectively.

To represent the viscous nature of a soft viscoelastic material, we will use the framework of dynamic viscosities, as given in Eq. (1). We define a set of dynamic viscosities for reporting the viscous or dissipative response in a similar fashion to the framework of the previous section. The definitions are

$$\eta_M' \equiv \left.\frac{d\sigma}{d\dot{\gamma}}\right|_{\dot{\gamma}=0} = \frac{1}{\omega}\sum_{n\ \text{odd}} nG_n''\left(-1\right)^{n-1/2} = v_1 - 3v_3 + \ldots \tag{8}$$

$$\eta_L' \equiv \left.\frac{\sigma}{\dot{\gamma}}\right|_{\dot{\gamma}=\dot{\gamma}_0} = \frac{1}{\omega}\sum_{n\ \text{odd}} G_n'' = v_1 + v_3 + \ldots \tag{9}$$

where η_M' is the *minimum-rate dynamic viscosity* and η_L' is the *large-rate dynamic viscosity*. These measures are represented graphically in FIG. 3b (linear response) and FIG. 3d (nonlinear response). Note that each measure of dynamic viscosity reduces to $\eta' = G''/\omega$ when the response is a single harmonic, i.e. $\eta_L' = \eta_M' = \eta_1' = \eta'(\omega)$ in the linear regime.

3. Dimensionless index of nonlinearity

These new alternative measures of elastic modulus and dynamic viscosity can be compared to quantify intra-cycle nonlinearities which distort the linear viscoelastic ellipse. For example, if the

large-strain modulus G'_L is greater than the minimum-strain modulus G'_M, then the response is strain-stiffening within the particular cycle (i.e. intra-cycle strain-stiffening). We define the following *strain-stiffening ratio* :

$$S \equiv \frac{G'_L - G'_M}{G'_L} = \frac{4e_3 + ...}{e_1 + e_3 + ...}. \tag{10}$$

Note that $S = 0$ for a linear elastic response, $S > 0$ indicates intra-cycle strain-stiffening, and $S < 0$ corresponds to intra-cycle strain-softening. Users of this framework may also choose to compare the moduli using e.g. the ratio $G'_L / G'_M = \left(1 - S\right)^{-1}$; we prefer the measure in Eq. (10) for convenience in relating the new measure to higher order Fourier/Chebyshev coefficients, and to eliminate potential singularities as $G'_M \to 0$.

We similarly define the *shear-thickening ratio* as

$$T \equiv \frac{\eta'_L - \eta'_M}{\eta'_L} = \frac{4v_3 + ...}{v_1 + v_3 + ...} \tag{11}$$

where $T = 0$ indicates a single harmonic linear viscous response, $T > 0$ represents intra-cycle shear-thickening, and $T < 0$ intra-cycle shear-thinning. The parameter T behaves in a comparable manner to the 3rd order viscous Chebyshev coefficient v_3, and therefore has a similar relationship to I_3 / I_1 and δ_3 as described at the end of Section II.A.

The full framework for characterizing nonlinear viscoelasticity is summarized in Table 1. The table includes both terminology and definitions of material measures.

III. MODEL EXAMPLES

In this section we illustrate and reinforce the interpretation of the new quantitative framework presented in Section II with some idealized model examples.

A. Purely elastic strain-stiffening solid

Consider a purely elastic solid material, whose shearing behavior can be represented by the constitutive expression

$$\begin{aligned} \sigma &= f(\gamma)\,\gamma \\ f(\gamma) &= G_0 + G_\beta \left(\frac{\gamma}{\gamma^*} \right)^2 \end{aligned} \tag{12}$$

where $f(\gamma)$ is the nonlinear elastic coefficient and γ^* is a critical strain beyond which nonlinear effects become significant. All nonlinear spring functions (e.g. FENE, wormlike chain, etc.) have leading order expansions of this form with expressions for G_β that vary with the chosen model; when G_β is positive the model is, by construction, strain-stiffening. It can be shown analytically (by using substitution and equating coefficients) that the decomposition of this nonlinear response results in the following elastic Chebyshev coefficients

$$\begin{aligned} e_1 &= G_1' = G_0 + \frac{3}{4}\left(\frac{\gamma_0}{\gamma^*} \right)^2 G_\beta \\ e_3 &= -G_3' = +\frac{1}{4}\left(\frac{\gamma_0}{\gamma^*} \right)^2 G_\beta . \end{aligned} \tag{13}$$

All higher coefficients $(e_5, e_7, ...)$ are zero as the function in Eq. (12) can be expressed exactly by the first two Chebyshev polynomials. As we expect for elastic strain-stiffening, e_3 is positive. However, because of the functional form of the Chebyshev basis functions the material nonlinearity corresponding to G_β is distributed between the first and third order terms. Accordingly, the first

harmonic Fourier component G_1' in fact represents a combination of both the zero-strain elastic modulus and a contribution from this nonlinear term [Walters (1975)]. In the limit of small imposed strain amplitudes, $\gamma_0 \ll \gamma^*$, $e_1 = G_1' \to G_0$ and $e_3 \to 0$ as we expect. It is clear that the first Chebyshev coefficient $e_1 = G_1'$ could be used to indicate inter-cycle stiffening if multiple data points were plotted against strain amplitude, but the degree of intra-cycle strain-stiffening is immediately apparent from one data point as indicated by the sign of e_3. It is also noteworthy that the third order Chebyshev and Fourier coefficients contain only 1/4 of the total nonlinear contribution to the stress amplitude. Thus, simply considering the magnitude of the third harmonic (e_3 or e_3/e_1) significantly underestimates the actual nonlinear contribution to the material response.

In contrast to the first-order Fourier elastic modulus, the alternative measures for reporting elastic modulus, G_M' and G_L', distinctly capture the small-strain elasticity $f(\gamma \to 0)$ and the large-strain elasticity $f(\gamma \to \gamma_0)$, respectively. That is,

$$G_M' = \sum_{n\,\text{odd}} nG_n' = e_1 - 3e_3 = G_0 \tag{14}$$

$$G_L' = \sum_{n\,\text{odd}} G_n' (-1)^{n-1/2} = e_1 + e_3 = G_0 + \left(\frac{\gamma_0}{\gamma^*}\right)^2 G_\beta. \tag{15}$$

Thus, the minimum-strain modulus $G_M' = f(\gamma = 0)$ equates to the zero-strain elasticity, whereas the large-strain modulus $G_L' = f(\gamma = \gamma_0)$ captures the large strain elasticity. Furthermore, the strain-stiffening ratio S correctly captures the true relative magnitude of the intra-cycle strain-stiffening,

$$S = \frac{\left(\frac{\gamma_0}{\gamma^*}\right)^2 G_\beta}{G_0 + \left(\frac{\gamma_0}{\gamma^*}\right)^2 G_\beta} \tag{16}$$

where $S \to 0$ in the limit of $\gamma_0 \ll \gamma^*$.

This simple example demonstrates how the interpretation of these new elastic material measures extract the key features of a nonlinear elastic response, and they can now be applied to any unknown material or constitutive model.

B. Purely viscous shear-thinning fluid

We next consider a purely viscous, but nonlinear, constitutive equation represented by

$$\sigma = g(\dot{\gamma})\,\dot{\gamma}$$
$$g(\dot{\gamma}) = \eta_0 - \eta_\beta \left(\frac{\dot{\gamma}}{\dot{\gamma}^*} \right)^2 \tag{17}$$

where $\dot{\gamma}^*$ is a critical strain-rate for shear-thinning to appear. This constitutive equation for shear stress is that of a generalized Newtonian fluid (GNF) and in particular it is an example of a Third-Order Fluid in simple shear [Bird *et al.* (1987)]. Any GNF model (in which viscosity can be written as a function of shear-rate) has a Taylor series expansion in the form of Eq. (17). For example the Carreau model for the viscosity coefficient has the following expression for $g\left(\dot{\gamma}\right)$ and associated Taylor expansion

$$g\left(\dot{\gamma}\right) = \eta_\infty + \left(\eta_0 - \eta_\infty\right)\left[1 + \left(\frac{\dot{\gamma}}{\dot{\gamma}^*}\right)^2\right]^{\frac{n-1}{2}} \simeq \eta_0 - \frac{1-n}{2}\left(\eta_0 - \eta_\infty\right)\left(\frac{\dot{\gamma}}{\dot{\gamma}^*}\right)^2 + \ \ldots \tag{18}$$

Eq. (17) is only intended to represent the initial deviation from linear behavior observed in a real material. It applies only for small values of $\dot{\gamma}_0$ such that shear stress is always monotonically increasing with shear-rate, i.e. $d\sigma/d\dot{\gamma} > 0$. This constrains the upper limit of oscillatory shear-rate amplitude in this example to values $\dot{\gamma}_0 < \dot{\gamma}^* \left(\eta_0/3\eta_\beta\right)^{1/2}$.

Applying the Chebyshev decomposition of Eq. (3) to Eq. (17) results in the following viscous material coefficients

$$\begin{aligned} v_1 &= \eta_1' = \eta_0 - \frac{3}{4}\eta_\beta \left(\frac{\dot{\gamma}_0}{\dot{\gamma}^*}\right)^2 \\ v_3 &= \eta_3' = -\frac{1}{4}\eta_\beta \left(\frac{\dot{\gamma}_0}{\dot{\gamma}^*}\right)^2 . \end{aligned} \tag{19}$$

As we expect, for shear-thinning the 3rd order viscous Chebyshev coefficient v_3 is negative. Again, the nonlinearity is distributed between the first and third order terms, whereas the alternative measures for reporting the first order viscous contribution, η_M' and η_L', distinctly represent the instantaneous zero-rate and maximum-rate viscosities, respectively

$$\eta_M' = \frac{1}{\omega}\sum_{n\ \text{odd}} nG_n''(-1)^{n-1/2} = v_1 - 3v_3 = \eta_0 \tag{20}$$

$$\eta_L' = \frac{1}{\omega}\sum_{n\ \text{odd}} G_n'' = v_1 + v_3 = \eta_0 - \eta_\beta \left(\frac{\dot{\gamma}_0}{\dot{\gamma}^*}\right)^2 . \tag{21}$$

Thus, the minimum-rate dynamic viscosity accurately captures the viscous material coefficient at zero shear-rate, $\eta_M' = g(\dot{\gamma} = 0) = \eta_0$ (i.e. the zero-shear rate viscosity), whereas the large-strain-rate dynamic viscosity represents the viscous material coefficient at maximum strain-rate, $\eta_L' = g(\dot{\gamma} = \dot{\gamma}_0)$. Finally, the shear-thickening index equates to

$$T = \frac{\eta_L' - \eta_M'}{\eta_L'} = \frac{-\eta_\beta \left(\frac{\dot{\gamma}}{\dot{\gamma}^*}\right)^2}{\eta_0 - \eta_\beta \left(\frac{\dot{\gamma}}{\dot{\gamma}^*}\right)^2} \tag{22}$$

which will have a negative value for a shear-thinning fluid. As we noted above, these new viscous material measures can now be applied to any unknown material or constitutive model.

C. Nonlinear Viscoelastic Model

The purely elastic and purely viscous models above can be superposed to construct a nonlinear model of Kelvin-Voigt form, $\sigma = f(\gamma)\gamma + g(\dot{\gamma})\dot{\gamma} = \sigma' + \sigma''$. For this simple nonlinear viscoelastic solid model, the elastic and viscous contributions will decompose exactly as shown previously, since the geometrical interpretation (stress decomposition) is immediately apparent by construction. To look beyond the simple decomposition of a nonlinear Kelvin-Voigt model we consider a prototypical nonlinear viscoelastic constitutive equation such as the Giesekus model which is commonly used for constitutive modeling of nonlinear viscoelastic fluids (see for example [Li *et al.* (1998); Yao *et al.* (1998)]). We examine the output of numerical simulations of this model in LAOS flow to illustrate our new interpretation and nomenclature (intra- and inter-cycle nonlinearities, stiffening/softening, and thickening/thinning) with the application of the Chebyshev decomposition and 2-D Pipkin diagrams.

The constitutive equation for the Giesekus model, as presented by Bird *et al.* (1987), is given by

$$\begin{aligned} \boldsymbol{\sigma} &= \boldsymbol{\sigma}_s + \boldsymbol{\sigma}_p \\ \boldsymbol{\sigma}_s &= \eta_s \dot{\boldsymbol{\gamma}} \\ \boldsymbol{\sigma}_p &+ \lambda_1 \boldsymbol{\sigma}_{p(1)} + \alpha \frac{\lambda_1}{\eta_p} \left\{ \boldsymbol{\sigma}_p \cdot \boldsymbol{\sigma}_p \right\} = \eta_p \dot{\boldsymbol{\gamma}}. \end{aligned} \tag{23}$$

Here $\boldsymbol{\sigma}_s$ is the solvent stress tensor, $\boldsymbol{\sigma}_p$ is the polymer stress tensor, $\boldsymbol{\sigma}_{p(1)}$ is the upper convected time derivative of the polymer stress, η_s is the solvent viscosity, η_p is the polymer viscosity, λ_1 is the relaxation time, and α is the mobility factor which gives rise to a nonlinear viscoelastic response (for $\alpha \neq 0$). In the linear viscoelastic regime, the Giesekus model reduces to the linear Jeffreys

model. The mechanical analog of the Jeffreys model is a Maxwell element representing the polymer (i.e. a spring in series with dashpot) in parallel with a Newtonian solvent (dashpot).

The Giesekus model was simulated under imposed oscillatory simple shear strain, $\gamma_{yx} = \gamma_0 \sin \omega t$, across a range of frequencies and strain amplitudes using the following model parameters, $\lambda_1 = 1\ \mathrm{s}$, $\eta_s = 0.01\ \mathrm{Pa.s}$, $\eta_p = 10\ \mathrm{Pa.s}$, and $\alpha = 0.3$. These four independent parameters result in a retardation time scale $\lambda_2 = \lambda_1 \eta_s / (\eta_s + \eta_p) = 0.001\ \mathrm{s}$ and a polymer shear modulus $G = \eta_p / \lambda_1 = 10\ \mathrm{Pa}$. The coupled system of differential equations was solved numerically with MATLAB for the range of $De_1 = \lambda_1 \omega = [10^{-2}, 10^3]$ and $\gamma_0 = [10^{-3}, 10]$. The 'ode15s' multistep solver was used with relative and absolute tolerances of 10^{-10}, and a maximum time step $t_{\max} = (0.004) 2\pi / \omega$ to ensure at least 250 points per cycle. Integration was continued until a steady oscillatory response was achieved (the shorter of $t = 18\lambda_1$ or $N = 1000$ cycles). For analysis of viscoelastic parameters, the final 10 oscillation periods were used (see Section IV.A.3 Data filtering and processing). The nonlinear term involving α in the polymer stress equation contributes to rich phase behavior in the 2-dimensional $\{\omega, \gamma_0\}$ parameter space (i.e. the Pipkin space). Material measures can be plotted as surfaces or contours within the Pipkin diagram [Thurston (1981); Thurston and Pope (1981); Giacomin and Oakley (1992); Reimers and Dealy (1996); Reimers and Dealy (1998)]. Two dimensional rheological fingerprints of the Giesekus model, as represented by contour plots of G_1', η_1', e_3/e_1, v_3/v_1, and I_3/I_1 are given in the Pipkin diagrams of FIG. 5.

The linear viscoelastic regime is indicated first by the vertical contour lines in FIG. 5a,b which show that G_1' and η_1' are independent of strain amplitude γ_0. The linear regime is more strictly confirmed by FIG. 5c,d,e which show the regions in which e_3/e_1, v_3/v_1, and I_3/I_1 are

negligibly small. We utilize a linear scale for e_3/e_1 and v_3/v_1 to emphasize the sign of the nonlinearity which is needed for a physical interpretation. It is observed that e_3/e_1 and v_3/v_1 are more sensitive indicators of material nonlinearities than I_3/I_1, since the third-order Chebyshev coefficients reach values of 0.001 at smaller strain amplitudes. The lower sensitivity of I_3/I_1 is attributed to the comparison of the total nonlinearity with the total magnitude of the fundamental harmonic, which allows a nonlinear subdominant component to be masked by a linear dominant component, e.g. a finite e_3/e_1 may be obscured if $v_1\omega \gg e_1$, since $I_3/I_1 = \sqrt{e_3+v_3\omega}\,\big/\sqrt{e_1+v_1\omega}$.

The linear viscoelastic (Jeffreys-like) response of the Giesekus model is observed for sufficiently small strain amplitude γ_0. In FIG. 5a the elastic modulus $G_1'(\omega,\gamma_0)$ plateaus at the value of the polymer modulus ($G_1' \to G = 10$ Pa) for $De_1 = \lambda_1\omega \gg 1$, $\gamma_0 \ll 1$. In FIG. 5b the low frequency dynamic viscosity plateaus at the total steady viscosity $\eta_1' \to \eta_s + \eta_p = 10.01$ Pa ($De_1 = \lambda_1\omega \ll 1$, $\gamma_0 \ll 1$). At sufficiently high frequencies ($De_1 = \lambda_1\omega \gg 1$, $\gamma_0 \ll 1$) we expect only the solvent viscosity to contribute to the dissipation, such that $\eta_1' \to \eta_s = 0.01$ Pa.s, which is shown by the lower plateau for η_1' in this region.

The boundary demarcating the limits of the linear regime is a function of frequency, as clearly seen from the contour plots in FIG. 5. For example, the linear viscoelastic regime extends to larger strain amplitudes γ_0 at lower frequencies. Indeed, at sufficiently low frequency one would expect a viscoelastic fluid to be dominated by its viscous characteristics. Thus nonlinearities at low frequency are triggered by a critical strain-rate amplitude $\dot{\gamma}_0$, rather than strain amplitude γ_0. Lines of constant strain-rate amplitude, such that $\dot{\gamma}_0 = \gamma_0\omega = \text{constant}$, would appear as diagonal lines of slope=-1 from the upper left to the lower right of the Pipkin diagrams in FIG. 5. The contours of

the first-order dynamic viscosity η_1' (FIG. 5b) reflect this response and show that a critical strain-rate triggers nonlinear effects at low frequency ($De_1 < 1$). At these low frequencies the viscous nonlinearities of the Giesekus model become apparent near a Weissenberg number $We_1 = \lambda_1 \omega \gamma_0 \lesssim 1$. Conversely, at higher frequency, $De_1 > 1$ when the fluid is dominated by elasticity, the nonlinear regime is determined by a critical strain amplitude γ_0, as seen by the horizontal contours in FIG. 5a ($De_1 \gg 1$).

The inter-cycle nonlinearities (i.e. the dependence of the material response on the imposed values of γ_0 or $\dot{\gamma}_0$), are indicated by the gradients of the contours in FIG. 5. Strain-softening results in a progressive decrease in the magnitude of the elastic modulus G_1' for strains $\gamma_0 > 1$ (FIG. 5a), i.e. the average elasticity decreases with strain-amplitude. This softening occurs more readily at higher frequencies. The fact that the contours of $G_1'(\omega, \gamma_0)$ are not self similar is an indication that the relaxation modulus of the Giesekus model cannot be written in a time-strain separable form, i.e. $G_1'(\omega, \gamma_0) \neq G'(\omega) h(\gamma_0)$ [Larson (1988)]. FIG. 5b captures the inter-cycle nonlinearity of the average viscous dissipation, showing inter-cycle shear-thinning of η_1' . Inter-cycle shear-thinning is not observed in the higher frequency regime, presumably because at sufficiently high frequencies only the Newtonian solvent dissipates energy and the viscous response becomes linear once more (i.e. $|v_3 / v_1| < 10^{-3}$), even for large amplitudes up to $\gamma_0 = 10$.

The contours of the normalized third-order Chebyshev coefficients e_3 / e_1 and v_3 / v_1 (FIG. 5c,d) give deeper insight into the viscoelastic nonlinearities of the Giesekus model. At any given location $\{\omega, \gamma_0\}$ in the Pipkin diagram, these Chebyshev coefficients quantify the intra-cycle nonlinearities (i.e. the nonlinearities in the material response within a steady oscillatory cycle). Elastic nonlinearities are revealed in FIG. 5c where regions of both intra-cycle strain-stiffening and

intra-cycle strain-softening are present, as indicated by the sign of e_3/e_1 being positive or negative, respectively. Intra-cycle strain-softening is predominant at higher frequency. The onset of this strain-softening appears to be mediated primarily by the strain-amplitude at the highest frequencies, as shown by the nearly horizontal contours of e_3/e_1 at high frequency. Intra-cycle stiffening is observed at moderate to low frequencies, creating a region where the sign of e_3/e_1 must change from negative to positive. Thus, a contour of $e_3/e_1 = 0$ exists at large strain-amplitudes, showing that an individual oscillatory response may appear to be linearly elastic even deep into the nonlinear viscoelastic regime. To fully explore viscoelastic material nonlinearity it is thus essential to perform a full series of frequency and strain amplitude sweeps. The intra-cycle viscous nonlinearities of FIG. 5d show two regions of intra-cycle shear-thinning ($v_3/v_1 < 0$) and one region of intra-cycle shear-thickening ($v_3/v_1 > 0$). This necessitates two transition regions where v_3/v_1 changes sign, again demonstrating that even at large amplitudes the intra-cycle response can be linearly viscous.

The Giesekus model response is determined by four model parameters ($G, \lambda_1, \alpha, \eta_s$). However, the response to a range of deformations $\{\omega, \gamma_0\}$ is not immediately apparent from inspection of the constitutive equation and knowledge of the values of these parameters. We have used our new framework (physically meaningful measures of nonlinearity, contour plot "fingerprints" of the material coefficients, and unambiguous nomenclature) to characterize the response of the Giesekus model under imposed oscillatory shear deformation, and can smoothly map the steady flow, linear viscoelastic, and nonlinear viscoelastic response. Our framework is able to describe the nonlinear viscoelastic response in general terms, i.e. without *a priori* knowledge of the material behavior in LAOS. Thus, the scheme can be applied to both constitutive models and experimental data, providing physically meaningful measures for comparison. Furthermore, the physical insight gained from examining experimental data in this way may help motivate the

selection of an appropriate constitutive model. We now proceed by using our new framework to describe experimental measurements of the material response in two representative complex fluids.

IV. EXPERIMENTAL EXAMPLES

To illustrate the experimental utility of our proposed new framework for describing LAOS tests, we apply it to data taken with a wormlike micellar solution and a natural biopolymeric hydrogel, gastropod pedal mucus. These analytic techniques may be applied to any rheologically complex material that is subjected to oscillatory simple shearing deformation.

A. Materials and methods

1. Materials

Slugs were collected in Cambridge, MA, kept in an indoor terrarium maintained at room temperature, and supplied with a diet of green leaf lettuce. Pedal mucus was collected by placing a slug on a glass plate and enticing it to crawl with a piece of food. Trail mucus was collected after the slug had crawled more than one body length to ensure that no debris remained in the sample.

The wormlike micelle solution (prepared as in Bhardwaj *et al.* (2007)) consists of cetylpyridinium chloride (CPyCl) and sodium salicylate (NaSal) dissolved in brine. The ratio of CPyCl/NaSal is 100 mM/50 mM (3.2 wt%/0.76 wt%) in a 100 mM (0.56 wt%) NaCl aqueous solution.

2. Data acquisition

All experiments were performed on a strain-controlled ARES rheometer (TA Instruments) equipped with a Peltier plate maintained at T=22ºC, using a solvent trap to inhibit evaporation. The pedal mucus was tested with a plate-plate geometry (diameter $D = 8$ mm, gap $h = 550$ μm). To

eliminate slip, the plate-plate surfaces were covered with adhesive-backed waterproof sandpaper, 600 grit (ARC Abrasives Inc). The micellar solution was tested with a cone-plate geometry (diameter $D = 50\,\text{mm}$, cone angle $\alpha = 0.0402\,\text{rad} = 2.30^\circ$, trunctation $48.8\ \mu\text{m}$).

Our analysis requires raw strain and stress signals. However, the standard oscillatory test setup available from the instrument control software (TA Orchestrator software) does not capture raw stress and strain waveforms; it only outputs the calculated viscoelastic parameters such as "elastic modulus" G'. In order to capture the stress and strain waveforms under oscillation we used the Arbitrary Waveshape Test capability of the TA Orchestrator software. With this test procedure the user can specify an equation for the strain input, and the raw strain and stress waveforms are saved to a data file. Note that this test procedure is part of the standard software which accompanies every ARES rheometer, making the technique broadly accessible to ARES users. Another option for capturing the time series waveforms, on the ARES and also some other rheometers, is to connect to voltage outputs of torque and displacement. Although higher sampling rates and larger signal to noise ratios may be obtained by collecting oversampled raw voltage signals of torque and displacement output [van Dusschoten and Wilhelm (2001); Wilhelm (2002)], the Arbitrary Waveshape Test has the advantage of directly collecting stress and strain data (rather than voltages) and does not require additional hardware such as an Analog-to-Digital Converter. Maximum sampling rates of the Arbitrary Waveshape Test were adequate for our experiments, with a maximum sampling rate near 100 samples/s. Multiple steady-state waveforms were used for data analysis (typically 4 cycles) at each coordinate pair $\{\omega, \gamma_0\}$.

3. Data filtering and processing

In preparation for Fourier transform (FT) processing, strain and stress data signals were first trimmed to contain an integer number of cycles, N, by identifying the zero crossings of the strain

signal. The discrete FT operation further requires that the strain and stress signals have data points which are equally spaced in time. Linear time spacing was inherent in the data collected experimentally, as a result of the analog to digital converter within the rheometer. However, the numerical integration routines used for the Giesekus simulation utilized a variable time stepper, and consequently the output strain and stress signals were interpolated to create data with equal time spacing. The prepared data signals were then analyzed with the 'fft' function in MATLAB which returns the discrete Fourier transform of the input vector, from which the trigonometric Fourier coefficients were determined (note that a vector with 2^m data points is *not* required for this operation). The resulting Fourier spectrum contains discrete information for frequencies up to the Nyquist frequency $\omega_{Nyquist} = \omega_1 n/2$, where ω_1 is the imposed frequency and n is the number of data points per cycle, with a frequency resolution $\Delta\omega = \omega_1 / N$, where N is the integer number of cycles.

The trimmed strain signal has a small but finite phase lag (imaginary component), since the first data point is not identically zero but instead a small positive number. This phase lag of the strain signal must be considered for precisely calculating the Fourier coefficients G'_n , G''_n . These Fourier coefficients are then directly used to calculate viscoelastic parameters such as G'_M and G'_L . The Fourier coefficients are particularly convenient for calculating parameters such as the minimum-strain modulus G'_M . This parameter would otherwise need to be calculated as the slope of a line via numerical differentiation (FIG. 3), but the experimental error is substantially reduced by calculating tangent properties such as G'_M and η'_M from the odd-harmonic Fourier coefficients as shown in Eqs. (6) and (8). The Chebyshev coefficients, e_n, v_n are also calculated from the Fourier spectrum c.f. Eq. (4), since this avoids the multiple processing steps of stress decomposition (Eq. (2)),

followed by the determination of Chebyshev coefficients using numerical integration of the corresponding orthogonality relation (see Appendix) combined with Eq. (3).

The stress decomposition of Cho *et al.* (2005) is also conveniently calculated from the odd, integer Fourier coefficients using Eq. (2). This stress decomposition is typically calculated by using the "find-and-subtract" method given by the first portion of Eq. (2) [Cho *et al.* (2005); Kim *et al.* (2006)]. The find-and-subtract method is easily implemented with simulated data [Kim *et al.* (2006)], but is more difficult to use with real experimental data sets because of two principal difficulties. First, it is unlikely that the available set of data points will have the appropriate strain/strain-rate symmetry, which necessitates the use of local interpolation methods. Second, subtracting two individual data points (from a data series that has not been smoothed or filtered) results in amplification of random noise. Accordingly, the elastic stress $\sigma'(\gamma)$ and viscous stress $\sigma''(\dot{\gamma})$ curves may not appear as smooth lines, but rather as scatter plots. Thus, in contrast to the findings of Kim *et al.* (2006), we find that the discrete Fourier transform approach provides greater accuracy than the find-and-subtract methodology. Using the odd, integer Fourier coefficients to construct the individual elastic and viscous stress contributions (Eq. (2)) eliminates both the problem of interpolation and noise amplification, resulting in smooth processed data containing corresponding information from the entire periodic stress signal (one may also consider reconstructing the strain and total stress time data from the FT coefficients, and thereafter using the Cho et al. subtraction algorithm, but an identical output is more quickly obtained by directly using Eq. (2)). Strain and strain-rate signals are also constructed to have data points at spacing which corresponds to the stress decomposition signals; the first-harmonic coefficients of the strain signal are used for this reconstruction.

Furthermore, we construct a smoothed *total* stress signal by utilizing only the odd, integer-harmonic components, up to a cutoff frequency, c.f. Eq. (1). This process can be described as

applying a discrete comb filter to the raw data, allowing only particular frequency components to pass through to the smoothed stress signal. Frequency information corresponding to even-harmonics and non-integer harmonics are neglected in the signal reconstruction because they contain only random noise and are non-physical for a material response devoid of transients, dynamic wall slip, and secondary flows, as mentioned in Section I. Selecting a cutoff frequency removes the high frequency components of the signal in which noise obscures any real signal. The use of multiple cycles N input to the FFT allows for data averaging, and an increase in the signal to noise ratio [Wilhelm *et al.* (1999)]. This data averaging of multiple cycles contributes to the digital filter's ability to smooth the total stress signal.

B. Gastropod pedal mucus

The apparent contradiction of the data shown in FIG. 1 can be resolved by applying the framework introduced in Section II. As noted in Section I, and shown in FIG. 1, slug pedal mucus exhibits substantial intra-cycle strain-stiffening as suggested by the Lissajous-Bowditch curves of stress vs. strain (FIG. 1b), but the elastic modulus, as captured by the first harmonic coefficient G_1', is approximately flat when plotted against strain-amplitude γ_0 (FIG. 1a).

The inter-cycle variations of the elastic moduli are shown in FIG. 6a where we plot G_1', G_M', G_L' as a function of imposed strain amplitude γ_0. It can be seen that these measures converge in the linear regime (though G_M' suffers from more experimental noise at these low strain amplitudes). The onset of material nonlinearity is indicated by the divergence of these three different measures of elastic modulus as the strain amplitude increases. In this biopolymer gel G_M' decreases with γ_0 (softening at small strains), whereas G_L' first decreases then increases, i.e. the

large-strain elasticity of the network first softens then stiffens (see FIG. 6a). The first-harmonic elastic modulus G_1' falls between the two other measures, supporting its interpretation as an average measure of elasticity throughout the oscillatory cycle.

The intra-cycle nonlinearities which distort the familiar linear viscoelastic ellipse are also quantified (FIG. 6c,d). Both S and e_3 are positive at the largest strain amplitudes (FIG. 6c), indicating strain-stiffening. These indicators of nonlinearity should be equal to zero in the linear regime (c.f. Eq. (10)). We see that the parameter S suffers more from noise than e_3, due to the error in calculating G_M' which is in the denominator of the calculation for S. However, both measures clearly indicate a strain-stiffening deviation from linear elasticity, with both measures taking positive values for large strain-amplitudes. This rich behavior in the elastic response of the gel is revealed and physically described only by the use of the present framework.

From FIG. 6b it is apparent that the dissipation at small strain-rates η_M' increases with increasing $\dot{\gamma}_0$, whereas the dissipative nature at large strain-rates (represented by η_L') decreases from one cycle to the next. At small strain-amplitudes these quantities suffer from residual noise, with greater perturbations than observed with the elastic quantities since the viscous contribution to the measured signal is comparatively smaller and the gel is predominantly elastic at these strain-amplitudes. At sufficient strain-amplitude, however, the values converge with each other before the nonlinear regime is reached at strain-rate amplitudes $\dot{\gamma}_0 > 2\ s^{-1}$. In the nonlinear regime the measures clearly diverge, with an increasing value of η_M', a nearly constant η_1', and a slightly decreasing value of η_L'. This increase of η_M' suggests that at small instantaneous strain-rates (corresponding to strains close to the maximum strain γ_0) the deformed material becomes progressively more dissipative.

The intra-cycle nonlinear viscous measures T and v_3 (FIG. 6d) are both negative at large strain amplitudes, indicating intra-cycle shear-thinning. This is consistent with the fact that $\eta'_L < \eta'_M$ in the nonlinear regime. Again, the true rheological behavior of the nonlinear viscoelastic material could be ascertained only by using the present framework. Insights such as these will help guide constitutive model development, since a physical picture of the nonlinear response is now readily apparent.

The utility of elastic and viscous Chebyshev decomposition is illustrated further by showing a Lissajous-Bowditch plot at a single coordinate point $\{\omega = 3\,\text{rad.s}^{-1},\ \gamma_0 = 2.8\}$ for native pedal mucus (FIG. 7). The total and decomposed stresses are displayed in FIG. 7a and FIG. 7b against the strain and strain-rate respectively. Overlaid on these figures are the reconstructions of the elastic and viscous stresses using only the 1st and 3rd order contributions for each signal. In FIG. 7c and FIG. 7d we report the spectrum of the elastic and viscous Chebyshev coefficients, respectively. It can be seen that the 1st and 3rd order contributions describe the nonlinear curves fairly well, thus giving confidence that they represent the predominant departure from linearity.

C. Wormlike Micellar fluid

In small amplitude oscillatory shear (SAOS) the viscoelastic behavior of this CPyCl wormlike micelle solution is well described by a single mode Maxwell model with $\lambda_1 = 0.64\ \text{s}$, while in steady shear the solution shear bands at a critical stress of approximately $\sigma \approx 20\,\text{Pa}$ [Pipe *et al.* (2006)].

Here we test the micellar solution in LAOS under strain-controlled conditions. Tests are performed over a frequency range of $\omega = [0.15, 15]$ with three points per decade, and a strain-amplitude range $\gamma_0 = [0.0056,\ 10]$ with four points per decade. We first use Lissajous-Bowditch

curves to summarize the rich viscoelastic response of the material as a function of both frequency and strain-amplitude. These Lissajous-Bowditch curves allow a visual inspection of the response prior to applying our quantitative analytic techniques. A subset of the elastic Lissajous-Bowditch curves are shown in FIG. 8, and the corresponding viscous Lissajous-Bowditch curves are displayed in FIG. 9 (the full set of raw data, covering four tests per decade of imposed strain, is available in the Appendix). The individual orbits ($\sigma(t)$ vs. $\gamma(t)$ or $\sigma(t)$ vs. $\dot{\gamma}(t)$) are arranged in FIG. 8 and FIG. 9 so that they are centered about the independent coordinates $\{\omega, \gamma_0\}$ to form a Pipkin diagram [Pipkin (1972)] of the material response over a range of frequency and strain. The linear viscoelastic regime is approached at adequately small strains, and is indicated in both FIG. 8 and FIG. 9 by elliptical curves that are independent of imposed strain amplitude γ_0 while frequency ω is held constant. The data suffers from noise in the lower left portions of FIG. 8 and FIG. 9 when $\sigma_{\max} < 0.10$ Pa, i.e. maximum torque $T_{\max} < 3.3 \mu N.m$. The onset of material nonlinearity can be visually observed for strains $\gamma_0 \geq 1$, at which point the shapes of the curves change and the elastic and viscous stress contributions to the total stress each become progressively more nonlinear. The nature of the initial deviation from linearity depends on the frequency, creating an extremely rich nonlinear response. For example, at $\omega = 0.75$ rad.s^{-1} ($\omega < 1/\lambda_1$) the initial elastic departure from linearity is strain-stiffening, whereas at $\omega = 3.0$ rad.s^{-1} ($\omega > 1/\lambda_1$) the initial nonlinearity is strain-softening.

The elastic properties of the micellar fluid are shown as contour plots, or "rheological fingerprints," in the two-dimensional Pipkin diagram of FIG. 10, and the corresponding viscous properties are shown in FIG. 11. Essential characteristics of the expected Maxwell behavior in the linear viscoelastic regime can be seen from the monotonically increasing value of G_1' with frequency and the approach to a plateau modulus. Furthermore, the contour plots of the third order elastic

Chebyshev coefficient e_3 in FIG. 10d show contrasting nonlinear trends for low and high frequencies. For low frequencies, $\omega < 2$ rad.s^{-1}, the elastic nonlinearity is strain-stiffening with $e_3 > 0$, whereas for higher frequency the elastic nonlinearity is strain-softening with $e_3 < 0$. The values of e_3 in the nonlinear regime are consistent with our visual inspections of the elastic Lissajous-Bowditch curves in FIG. 8.

Reporting more than the common first-order viscoelastic moduli G_1' and $G_1'' = \eta_1'\omega$ also reveals behavior which might otherwise be hidden. The Lissajous-Bowditch curves of FIG. 8 and FIG. 9 show a curious behavior at $\{\omega = 0.75$ rad.s$^{-1}, \gamma_0 = 10\}$, in which self-intersection appears in the viscous Lissajous-Bowditch curves (leading to loops) and a negative slope appears in the elastic Lissajous-Bowditch curves at instantaneous strain value $\gamma = 0$. There is nothing in the contour plot of G_1' (FIG. 10c) or η_1' (FIG. 11c) which hints at such behavior; the contours of G_1' and η_1' appear unremarkable in this region of the Pipkin diagram. However, the small-strain elastic modulus G_M' takes a negative value at this point (FIG. 10a), which corresponds to the negative slope in the elastic Lissajous-Bowditch curve at $\gamma = 0$, and leads to the self-intersection in the viscous Lissajous-Bowditch curve. A negative modulus G_M' indicates that the material is unloading elastic stress faster than new deformation is being accumulated. This behavior can easily be hidden by the commonly reported viscoelastic parameters of G_1' or $G_1'' = \eta_1'\omega$, but is revealed quantitatively with the alternative measures of viscoelastic moduli proposed in this work.

The physical insight provided by these material measures informs a microstructural picture of the material, which in turn helps to motivate the choice of a constitutive model. Furthermore, these measures can be used to help test the robustness of a constitutive model, to see if the model is capable of predicting the same nonlinear response over a range of imposed strains and timescales.

V. CONCLUSIONS

The growing interest in nonlinear viscoelastic properties of biological networks and other soft materials compels a need for self-consistent, laboratory-independent, low-dimensional descriptions of nonlinear material responses. In this paper we have proposed a descriptive language and a set of unambiguous material measures which quantify nonlinear viscoelastic behavior in such a way. The scheme provides a physical interpretation of deviations from linear viscoelastic behavior, characterizing elastic and viscous nonlinearities separately, simultaneously, and more thoroughly than currently reported measures. In addition, the method can be easily applied to previously collected data using existing software[‡] or used to interpret previously reported FT rheology parameters.

In the future we hope to apply this framework to the study of many other complex fluids and soft solids, including biopolymer networks, foods, nano-composites, and concentrated suspensions. These new measures may lend insight in the development of appropriate constitutive models for describing nonlinear soft material, and may also serve as a more sensitive discriminator for comparing and contrasting different materials. It will also be of interest to investigate the characteristic rheological fingerprints of soft solids which exhibit a yield stress or critical stress. The resulting viscous and elastic Lissajous- Bowditch curves will be markedly different to those shown in the present studies (see e.g. Mujumdar *et al.* (2002)), and the yielding transition will in fact correspond to a specific yield envelope or critical value of $\{\omega, \gamma_0\}$ in the corresponding Pipkin diagram. For probing such materials it makes most sense to consider stress controlled tests with an

---

[‡] Software to analyze raw measurement of $\{\gamma(t), \sigma(t)\}$ is available from the authors or from http://web.mit.edu/nnf/

input stress of the form $\sigma(t) = \sigma_0 \cos(\omega t)$. We plan to explore the extension of the current framework to the quantitative description of stress-controlled tests.

The new framework presented herein is broadly applicable to any material which can be tested in oscillatory shear, including complex fluids and soft solids, and serves as a complement to the familiar and successful linear viscoelastic framework embodied in the familiar material functions $G'(\omega)$ and $G''(\omega)$. The new measures presented here will provide a more rigorous test of constitutive models, and serve as a sensitive probe for comparing and understanding the true nonlinear rheological properties of different materials.

ACKNOWLEDGEMENTS

The authors extend their thanks to T. S. K. Ng, R. J. Larsen, K. Hyun, and M. Wilhelm for helpful discussions, to N. J. Kim for help with the collection of slugs, and to N. J. Kim and C. J. Pipe for the preparation of the micellar solution. This research was supported in part by a gift from Procter & Gamble. R. H. E. acknowledges the National Science Foundation Graduate Research Fellowship for financial support.

APPENDIX

CHEBYSHEV POLYNOMIALS

The Chebyshev polynomials of the first kind are orthogonal over the domain [-1,1]. The n=0-5 order polynomials, along with the recursive definition are given below [Abramowitz and Stegun (1964)].

$$T_0(x)=1 \qquad T_4(x)=8x^4-8x^2+1$$
$$T_1(x)=x \qquad T_5(x)=16x^5-20x^3+5x$$
$$T_2(x)=2x^2-1 \qquad T_{n+1}(x)=2xT_x(x)-T_{n-1}(x)$$
$$T_3(x)=4x^3-3x$$

The orthogonality relation is given by

$$\int_{-1}^{1}\frac{T_m(x)T_n(x)}{\left(1-x^2\right)^{1/2}}dx = \begin{cases}\frac{1}{2}\pi & \text{for } m\neq 0, n\neq 0\\ \pi & \text{for } m=n=0\end{cases}.$$

In this work we also use the identity $T_n(\cos\theta)=\cos(n\theta)$. This can be used to derive the identity for $T_n(\sin\theta)$ by using $\sin\theta=\cos(\pi/2-\theta)$.

$$\begin{aligned}T_n(\sin\theta) &= T_n\left(\cos\left(\frac{\pi}{2}-\theta\right)\right)\\ &= \cos(n\pi/2-n\theta)\\ &= \cos(n\pi/2)\cos(n\theta)+\sin(n\pi/2)\sin(n\theta)\\ &= \begin{cases}\sin(n\theta)(-1)^{(n-1)/2} & n:\text{odd}\\ \cos(n\theta)(-1)^{n/2} & n:\text{even}\end{cases}\end{aligned}$$

Table 1. Material measures and nomenclature for characterizing nonlinear viscoelasticity with imposed oscillatory shear strain

Elastic Characterization

	Material Measures	Interpretation
Linear, first-order properties	$G_1' = \frac{\omega}{\pi\gamma_0^2}\oint\sigma(t)\gamma(t)dt$	First-harmonic (average) elastic modulus
	$G_M' \equiv \left.\frac{d\sigma}{d\gamma}\right\|_{\gamma=0}$	Minimum-strain elastic modulus
	$G_L' \equiv \left.\frac{\sigma}{\gamma}\right\|_{\gamma=\gamma_0}$	Large-strain elastic modulus
Nonlinear properties	$e_3 = -G_3'$	Intra-cycle *elastic* nonlinearities
	$S \equiv \frac{G_L' - G_M'}{G_L'} = \frac{4e_3 + \ldots}{e_1 + e_3 + \ldots}$	e_3 and/or S $\begin{cases} > 0 & \text{strain-stiffening} \\ = 0 & \text{linear elastic} \\ < 0 & \text{strain-softening} \end{cases}$

Viscous Characterization

	Material Measures	Interpretation
Linear, first-order properties	$\eta_1' = \frac{1}{\pi\omega\gamma_0^2}\oint\sigma(t)\dot{\gamma}(t)dt$	First-harmonic (average) dynamic viscosity
	$\eta_M' \equiv \left.\frac{d\sigma}{d\dot{\gamma}}\right\|_{\dot{\gamma}=0}$	Minimum-rate dynamic viscosity
	$\eta_L' \equiv \left.\frac{\sigma}{\dot{\gamma}}\right\|_{\dot{\gamma}=\dot{\gamma}_0}$	Large-rate dynamic viscosity
Nonlinear properties	$v_3 = G_3''/\omega$	Intra-cycle *viscous* nonlinearities
	$T \equiv \frac{\eta_L' - \eta_M'}{\eta_L'} = \frac{4v_3 + \ldots}{v_1 + v_3 + \ldots}$	v_3 and/or T $\begin{cases} > 0 & \text{shear-thickening} \\ = 0 & \text{linear viscous} \\ < 0 & \text{shear-thinning} \end{cases}$

Figure Captions

FIG. 1. Oscillatory strain sweeps of pedal mucus from *Limax maximus* at a frequency ω = 3 rad.s^{-1}. (a) Typical rheometer output of the fluid viscoelasticity as parameterized by the first-harmonic Fourier moduli; (b) Plotting the raw data from every-other point as $\sigma(t)$ vs. $\gamma(t)$ reveals additional nonlinear characteristics that are obscured by G_1', G_1''.

FIG. 2. Applying the geometrical interpretation of Cho *et al.* (2005) to the largest strain amplitude data point from FIG. 1, $\{\omega = 3 \text{ rad.s}^{-1}, \gamma_0 = 2.8\}$; (a) total stress and elastic stress σ', (b) total stress and viscous stress σ''.

FIG. 3. Definitions of new measures for reporting viscoelastic moduli: (a),(b) elastic moduli and dynamic viscosities, respectively, for a model linear viscoelastic response with $G' = 0.8$, $G'' = 0.6$ at $\{\omega = 1 \text{ rad.s}^{-1}, \gamma_0 = 1\}$; (c),(d) elastic moduli and dynamic viscosities, respectively, for a nonlinear viscoelastic response (experimental data shown is same as FIG. 2). The first harmonic moduli are shown for comparison. In the linear regime (a,b) all measures are equivalent to the linear viscoelastic moduli. A nonlinear material response (c,d) will result in different values for each material measure.

FIG. 4. Different elliptical approximations to a nonlinear viscoelastic signal, using the newly proposed alternative measures of elastic modulus.

FIG. 5. Pipkin diagram plots of resulting viscoelastic parameters for a simulated nonlinear viscoelastic fluid (Giesekus model, $\lambda_1 = 1$ s, $\eta_s = 0.01$ Pa.s, $\eta_p = 10$ Pa.s, and $\alpha = 0.3$); (a) first order elastic modulus G_1', contours shown at increments of 2 Pa (b) first order dynamic viscosity η_1', contours shown at increments of 2 Pa (c) normalized third-order elastic Chebyshev coefficient e_3/e_1, contours as labeled, (d) scaled third-order viscous Chebyshev coefficient v_3/v_1, contours shown at ±0.001, ±0.025, ±0.05, ±0.1, +0.15, and (e) normalized intensity of the third harmonic $I_3/I_1 = |G_3^*|/|G_1^*|$, contours shown at 0.001, and increments of 0.01.

FIG. 6. Oscillatory shear test of pedal mucus from FIG. 1, $\omega = 3$ rad.s^{-1}, analyzed within the new framework; (a) Elastic moduli: minimum-strain and large-strain elastic moduli compared to first harmonic elastic modulus (b) Dynamic viscosities: minimum-rate and large-rate dynamic viscosities compared to first harmonic dynamic viscosity, (c) Intra-cycle elastic nonlinearity measures: scaled 3rd order elastic Chebyshev coefficient e_3/e_1 and strain-stiffening ratio S, both indicate intra-cycle strain-stiffening; (d) Intra-cycle measures of viscous nonlinearity: 3rd order viscous Chebyshev coefficient v_3/v_1 and shear-thickening ratio T, both indicate intra-cycle shear-thinning. Error bars are determined from the noise in the Fourier spectrum and are shown for representative points. The data point size exceeds the error margins at larger amplitudes. For e_3/e_1 and v_3/v_1 (star symbols) the data point size exceeds the error for all amplitudes.

FIG. 7. Reconstruction of (a) elastic and (b) viscous stresses using the Chebyshev spectrum of each signal (c,d). The nonlinearity of each signal is predominantly described by including only the third-order contribution; contributions higher than $n = 3$ are comparably insignificant ($e_5/e_1, v_5/v_1 < 0.005$) (same experimental data as FIG. 2).

FIG. 8. Elastic Lissajous-Bowditch curves generated from experimental oscillatory tests of the micellar solution, displayed in a Pipkin space. Each trajectory is positioned according to the imposed values $\{\omega, \gamma_0\}$. Solid lines are total stress (filtered) $\sigma(t)/\sigma_{\max}$ vs. $\gamma(t)/\gamma_0$, dashed lines are elastic stress $\sigma'(t)/\sigma_{\max}$ vs. $\gamma(t)/\gamma_0$. The maximum stress, $\sigma_{\max}$, is indicated above each curve.

FIG. 9. Viscous Lissajous-Bowditch curves generated from experimental oscillatory tests of the micellar solution, displayed in a Pipkin space. Each trajectory is positioned according to the imposed values $\{\omega, \gamma_0\}$. Solid lines are total stress (filtered) $\sigma(t)/\sigma_{\max}$ vs. $\dot{\gamma}(t)/\dot{\gamma}_0$, dashed lines are viscous stress $\sigma''(t)/\sigma_{\max}$ vs. $\dot{\gamma}(t)/\dot{\gamma}_0$. The maximum stress, $\sigma_{\max}$, is indicated above each curve.

FIG. 10. "Rheological Fingerprints" of the elastic properties of the micellar solution in large amplitude oscillatory shear. Each parameter is plotted in a Pipkin diagram as a function of the imposed frequency and strain amplitude. (a,b,c) Elastic moduli G'_M, G'_L, and G'_1 respectively; unlabeled contours shown at increments of 2 Pa (d) Intra-cycle elastic nonlinearity as indicated by the normalized third-order elastic Chebyshev term, e_3/e_1; contours shown at -0.05, ±0.01, and increments of 0.2.

FIG. 11. Viscous properties of the micellar solution in large amplitude oscillatory shear, each parameter plotted in a Pipkin space; (a,b,c) Dynamic viscosities η'_M, η'_L, and η'_1 respectively; contours shown at increments of 2 Pa.s. Inter-cycle nonlinearities are indicated by gradients of these measures. Inter-cycle thinning is shown for sufficiently large and increasing values of the shear rate amplitude $\dot{\gamma}_0 = \gamma_0\omega$. (d) Intra-cycle viscous nonlinearity as indicated by the normalized third-order viscous Chebyshev term, v_3/v_1; contours shown at increments of 0.05. Intra-cycle thickening is indicated by $v_3/v_1 > 0$, whereas intra-cycle thinning is shown by $v_3/v_1 < 0$.

Appendix FIG. A1: Chebyshev polynomials of the first kind; plots of the first few odd polynomials.

Appendix FIG. A2: Raw LAOS data for the micellar solution, shown as elastic Lissajous-Bowditch curves generated from experimental oscillatory tests. Each trajectory is positioned in a Pipkin space according to the imposed values $\{\omega, \gamma_0\}$. Solid lines are total stress $\sigma(t)/\sigma_{\max}$ vs. $\gamma(t)/\gamma_0$. The maximum stress, $\sigma_{\max}$, is indicated above each curve.

References

Abramowitz, M. and I. A. Stegun, *Handbook of Mathematical Functions with Formulas, Graphs, and Mathematical Tables* (Dover, New York, 1964)

Atalik, K. and R. Keunings, "On the occurrence of even harmonics in the shear stress response of viscoelastic fluids in large amplitude oscillatory shear," Journal of Non-Newtonian Fluid Mechanics **122**(1-3), 107-116 (2004)

Bhardwaj, A., E. Miller and J. P. Rothstein, "Filament stretching and capillary breakup extensional rheometry measurements of viscoelastic wormlike micelle solutions," Journal of Rheology **51**(4), 693-719 (2007)

Bird, R., R. Armstrong and O. Hassager, *Dynamics of Polymeric Liquids: Volume 1 Fluid Mechanics* (John Wiley & Sons, Inc, New York, 1987)

Chaudhuri, O., S. H. Parekh and D. A. Fletcher, "Reversible stress softening of actin networks," Nature **445**, 295-298 (2007)

Cho, K. S., K. H. Ahn and S. J. Lee, "A geometrical interpretation of large amplitude oscillatory shear response," Journal of Rheology **49**(3), 747-758 (2005)

Crowell, A. D., "Motion of the Earth as Viewed from the Moon and the Y-Suspended Pendulum," American Journal of Physics **49**(5), 452-454 (1981)

Dealy, J. M. and K. F. Wissbrun, *Melt rheology and its role in plastics processing : theory and applications* (Van Nostrand Reinhold, New York, 1990)

Debbaut, B. and H. Burhin, "Large amplitude oscillatory shear and Fourier-transform rheology for a high-density polyethylene: Experiments and numerical simulation," Journal of Rheology **46**(5), 1155-1176 (2002)

Dotsch, T., M. Pollard and M. Wilhelm, "Kinetics of isothermal crystallization in isotactic polypropylene monitored with rheology and Fourier-transform rheology," Journal of Physics: Condensed Matter **15**(11), S923-S931 (2003)

Ewoldt, R. H., C. Clasen, A. E. Hosoi and G. H. McKinley, "Rheological fingerprinting of gastropod pedal mucus and synthetic complex fluids for biomimicking adhesive locomotion," Soft Matter **3**(5), 634-643 (2007)

Ferry, J. D., *Viscoelastic properties of polymers* (Wiley, 1980)

Ganeriwala, S. N. and C. A. Rotz, "Fourier-Transform Mechanical Analysis For Determining The Nonlinear Viscoelastic Properties Of Polymers," Polymer Engineering and Science **27**(2), 165-178 (1987)

Gardel, M. L., J. H. Shin, F. C. MacKintosh, L. Mahadevan, P. Matsudaira and D. A. Weitz, "Elastic behavior of cross-linked and bundled actin networks," Science **304**(5675), 1301-1305 (2004)

Giacomin, A. J. and J. M. Dealy (1993). Large-Amplitude Oscillatory Shear, in Techniques in rheological measurement. A. A. Collyer. London, Elsevier Applied Science, Ch. 4

Giacomin, A. J. and J. G. Oakley, "Structural network models for molten plastics evaluated in large-amplitude oscillatory shear," Journal of Rheology **36**(8), 1529-1546 (1992)

Gisler, T., R. Ball and D. A. Weitz, "Strain hardening of fractal colloidal gels," Physical Review Letters **82**(5), 1064-1067 (1999)

Graham, M. D., "Wall Slip And The Nonlinear Dynamics Of Large-Amplitude Oscillatory Shear Flows," Journal of Rheology **39**(4), 697-712 (1995)

Janmey, P. A., E. J. Amis and J. D. Ferry, "Rheology Of Fibrin Clots .6. Stress-Relaxation, Creep, And Differential Dynamic Modulus Of Fine Clots In Large Shearing Deformations," Journal of Rheology **27**(2), 135-153 (1983)

Kim, H., K. Hyun, D. J. Kim and K. S. Cho, "Comparison of interpretation methods for large amplitude oscillatory shear response," Korea-Australia Rheology Journal **18**(2), 91-98 (2006)

Klein, C., H. W. Spiess, A. Calin, C. Balan and M. Wilhelm, "Separation of the nonlinear oscillatory response into a superposition of linear, strain hardening, strain softening, and wall slip response," Macromolecules **40**(12), 4250-4259 (2007)
Klein, C., P. Venema, L. Sagis and E. van der Linden, "Rheological discrimination and characterization of carrageenans and starches by Fourier transform-rheology in the non-linear viscous regime," Journal of Non-Newtonian Fluid Mechanics **151**(1-3), 145-150 (2008)
Larson, R. G., *Constitutive equations for polymer melts and solutions* (Butterworths, Boston, 1988) Ch. 6
Li, J. M., W. R. Burghardt, B. Yang and B. Khomami, "Flow birefringence and computational studies of a shear thinning polymer solution in axisymmetric stagnation flow," Journal of Non-Newtonian Fluid Mechanics **74**(1-3), 151-193 (1998)
Ma, L. L., J. Y. Xu, P. A. Coulombe and D. Wirtz, "Keratin filament suspensions show unique micromechanical properties," Journal of Biological Chemistry **274**(27), 19145-19151 (1999)
Mujumdar, A., A. N. Beris and A. B. Metzner, "Transient phenomena in thixotropic systems," Journal of Non-Newtonian Fluid Mechanics **102**(2), 157-178 (2002)
Neidhofer, T., M. Wilhelm and B. Debbaut, "Fourier-transform rheology experiments and finite-element simulations on linear polystyrene solutions," Journal of Rheology **47**(6), 1351-1371 (2003)
Philippoff, W., "Vibrational Measurements with Large Amplitudes," Transactions of the Society of Rheology **10**(1), 317-334 (1966)
Pipe, C. J., N. J. Kim and G. H. McKinley,"Investigating the steady and transient non-linear rheology of wormlike micellar solutions," 78th Annual Meeting of The Society of Rheology, Portland, ME, Paper GP7 (2006)
Pipkin, A. C., *Lectures on viscoelasticity theory* (Springer-Verlag, New York, 1972) viii, 180 p. illus. 26 cm.
Reimers, M. J. and J. M. Dealy, "Sliding plate rheometer studies of concentrated polystyrene solutions: Large amplitude oscillatory shear of a very high molecular weight polymer in diethyl phthalate," Journal of Rheology **40**(1), 167-186 (1996)
Reimers, M. J. and J. M. Dealy, "Sliding plate rheometer studies of concentrated polystyrene solutions: Nonlinear viscoelasticity and wall slip of two high molecular weight polymers in tricresyl phosphate," Journal of Rheology **42**(3), 527-548 (1998)
Spenley, N. A., M. E. Cates and T. C. B. McLeish, "Nonlinear rheology of wormlike micelles," Physical Review Letters **71**(6), 939-942 (1993)
Storm, C., J. J. Pastore, F. C. MacKintosh, T. C. Lubensky and P. A. Janmey, "Nonlinear elasticity in biological gels," Nature **435**(7039), 191-194 (2005)
Tee, T. T. and J. M. Dealy, "Nonlinear viscoelasticity of polymer melts," Transactions of the Society of Rheology **19**(4), 595-615 (1975)
Thurston, G. B., "Shear Rate Dependence of the Viscoelasticity of Polymer-Solutions. 1. Theoretical-Model," Journal of Non-Newtonian Fluid Mechanics **9**(1-2), 57-68 (1981)
Thurston, G. B. and G. A. Pope, "Shear Rate Dependence of the Viscoelasticity of Polymer-Solutions.2. Xanthan Gum," Journal of Non-Newtonian Fluid Mechanics **9**(1-2), 69-78 (1981)
van Dusschoten, D. and M. Wilhelm, "Increased torque transducer sensitivity via oversampling," Rheologica Acta **40**(4), 395-399 (2001)
Walters, K., *Rheometry* (Wiley, New York, 1975), p. 143
Wilhelm, M., "Fourier-Transform rheology," Macromolecular Materials and Engineering **287**(2), 83-105 (2002)
Wilhelm, M., P. Reinheimer and M. Ortseifer, "High sensitivity Fourier-transform rheology," Rheologica Acta **38**(4), 349-356 (1999)

Wyss, H. M., K. Miyazaki, J. Mattsson, Z. B. Hu, D. R. Reichman and D. A. Weitz, "Strain-rate frequency superposition: A rheological probe of structural relaxation in soft materials," Physical Review Letters **98**(23) (2007)

Yao, M. W., G. H. McKinley and B. Debbaut, "Extensional deformation, stress relaxation and necking failure of viscoelastic filaments," Journal of Non-Newtonian Fluid Mechanics **79**(2-3), 469-501 (1998)

Yao, N. Y., R. J. Larsen and D. A. Weitz, "Probing nonlinear rheology with inertio-elastic oscillations," Journal of Rheology(4), 1013-1025 (2008)

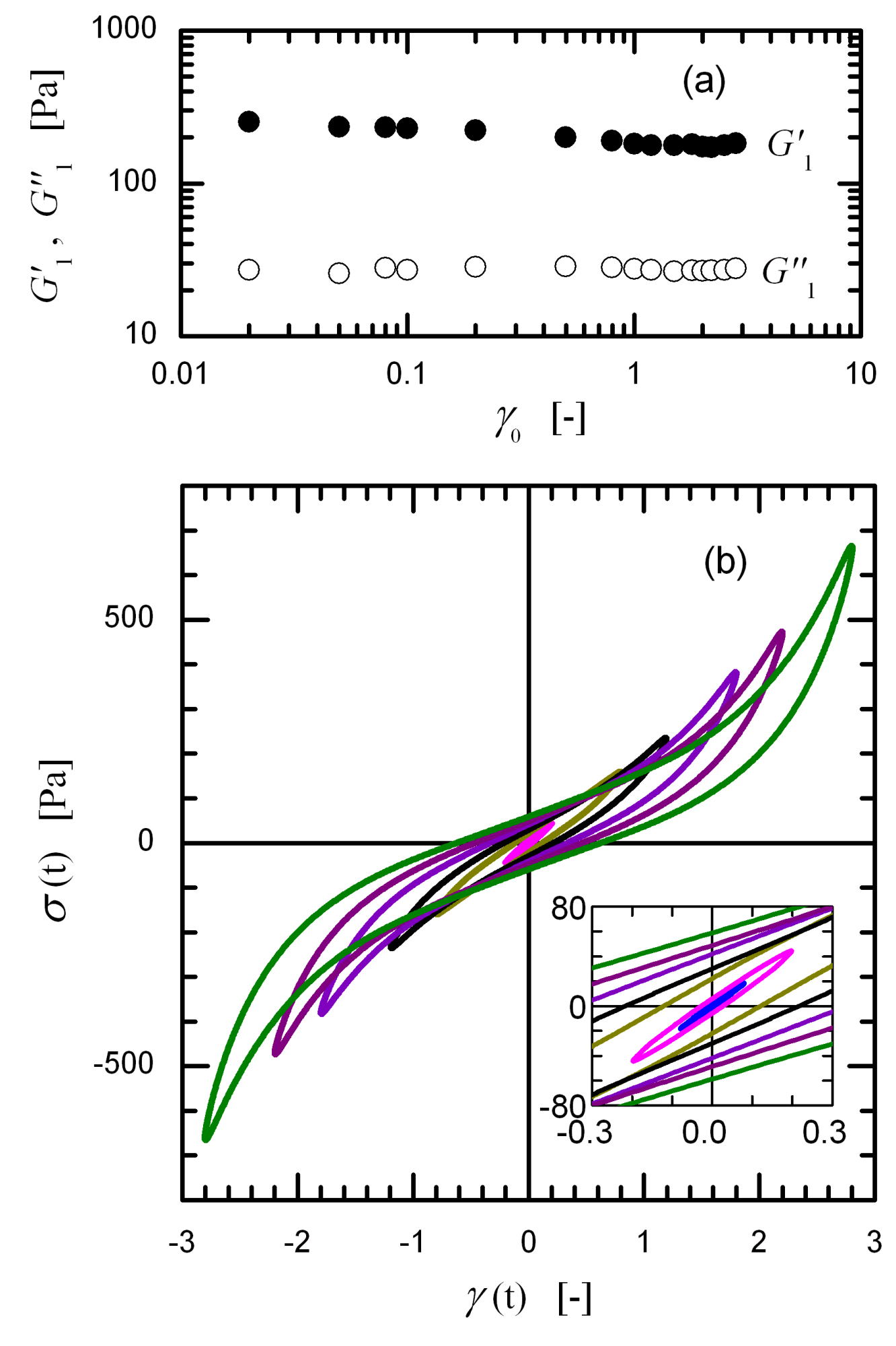
(a)
1000
100
10
0.01
0.1
1
10
G'_1 , G''_1 [Pa]
γ_0 [-]
G'_1
G''_1
(b)
500
0
-500
-3
-2
-1
0
1
2
3
σ(t) [Pa]
γ(t) [-]
80
0
-80
-0.3
0.0
0.3

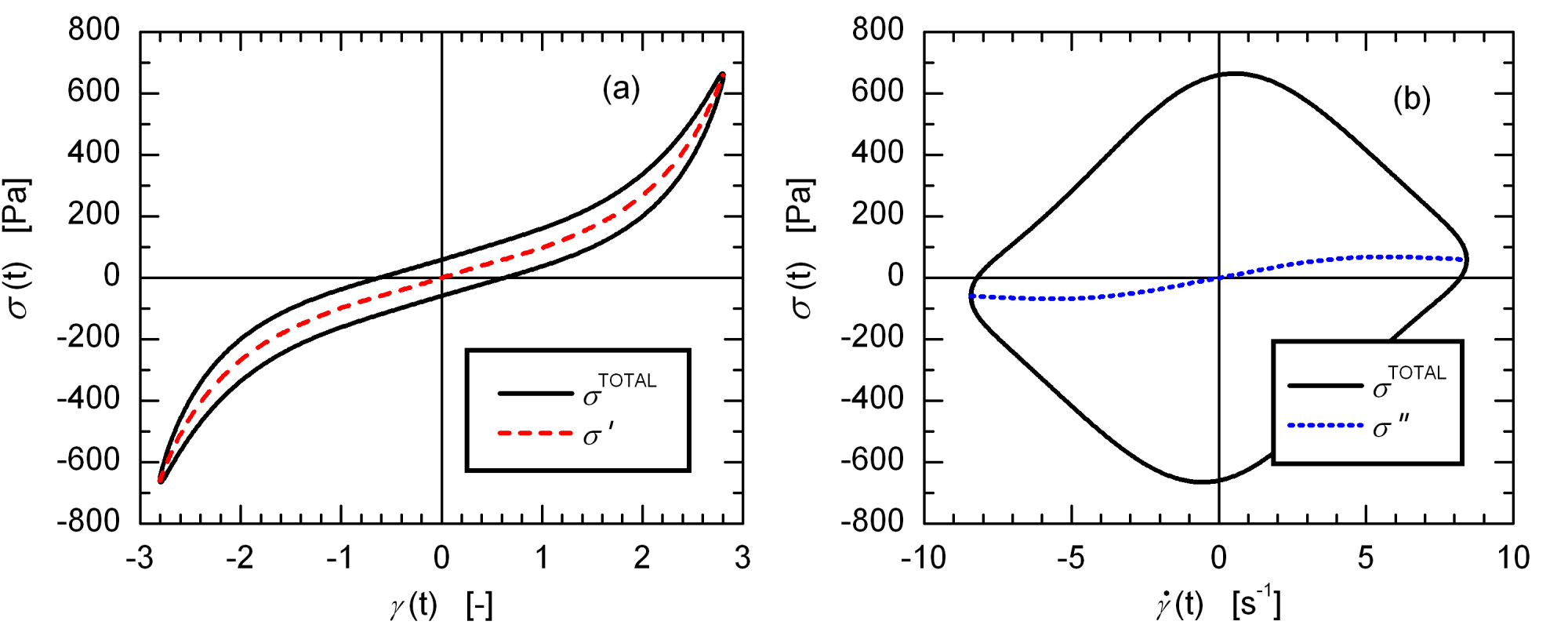
(a)
σ(t) [Pa]
γ(t) [-]
σ TOTAL
σ '
(b)
σ(t) [Pa]
γ̇(t) [s-1]
σ TOTAL
σ ''

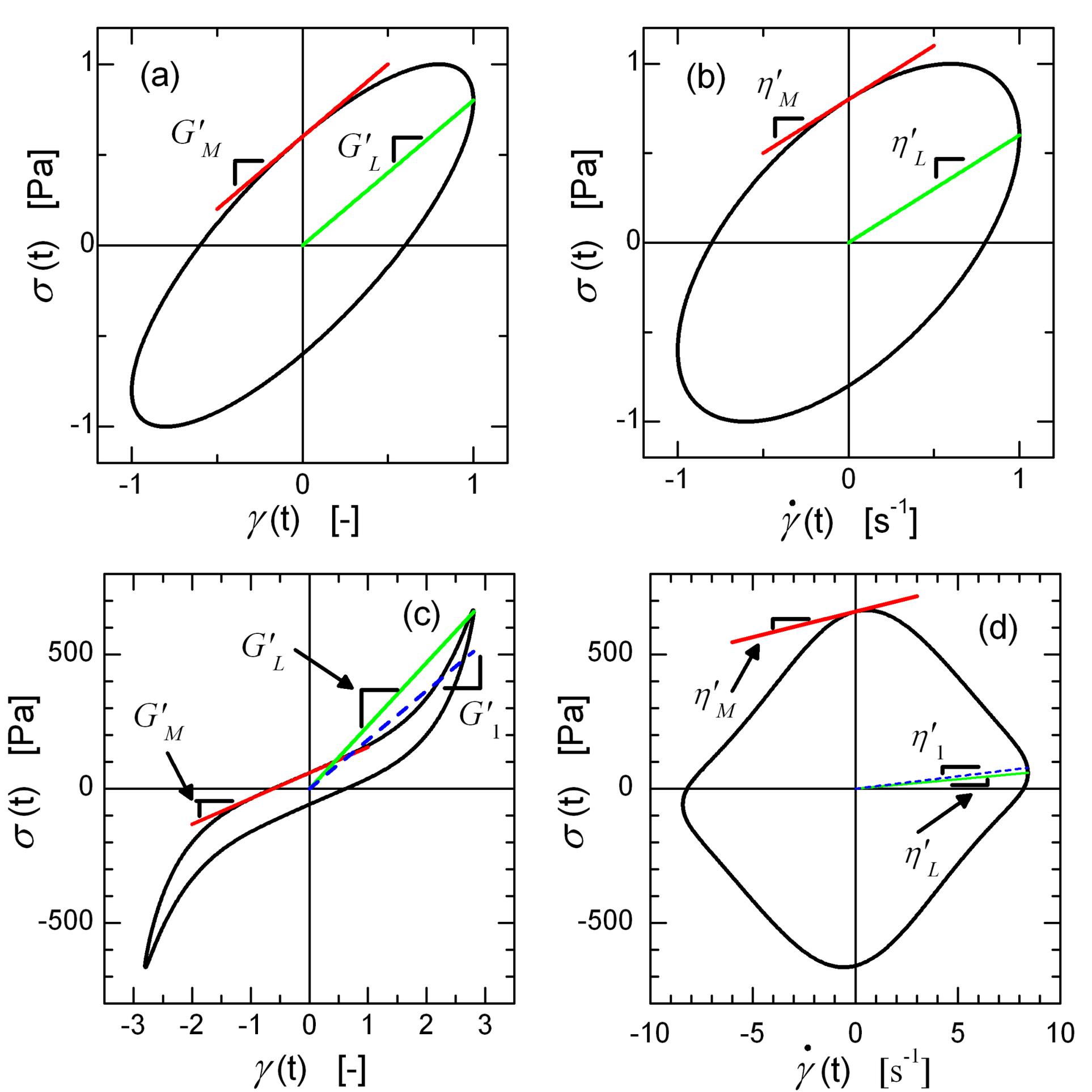
(a)
G'_M
G'_L
σ(t) [Pa]
γ(t) [-]
(b)
η'_M
η'_L
σ(t) [Pa]
$\dot{\gamma}$(t) [s^{-1}]
(c)
G'_L
G'_M
G'_1
σ(t) [Pa]
γ(t) [-]
(d)
η'_M
η'_1
η'_L
σ(t) [Pa]
$\dot{\gamma}$(t) [s^{-1}]

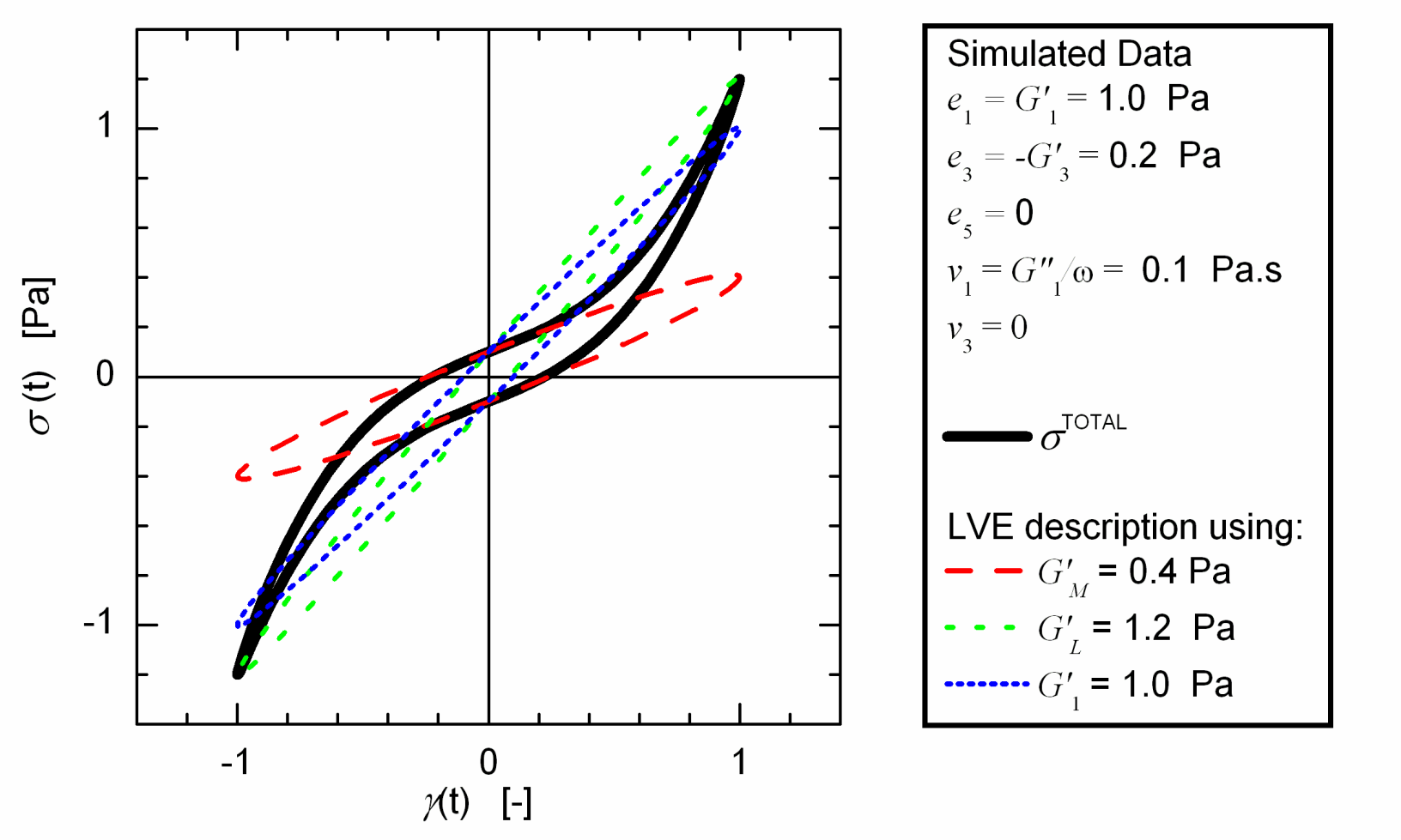
1
0
-1
σ (t) [Pa]
-1
0
1
γ(t) [-]
Simulated Data
$e_1 = G'_1 = 1.0$ Pa
$e_3 = -G'_3 = 0.2$ Pa
$e_5 = 0$
$v_1 = G''_1/\omega = 0.1$ Pa.s
$v_3 = 0$
σ^{TOTAL}
LVE description using:
$G'_M = 0.4$ Pa
$G'_L = 1.2$ Pa
$G'_1 = 1.0$ Pa

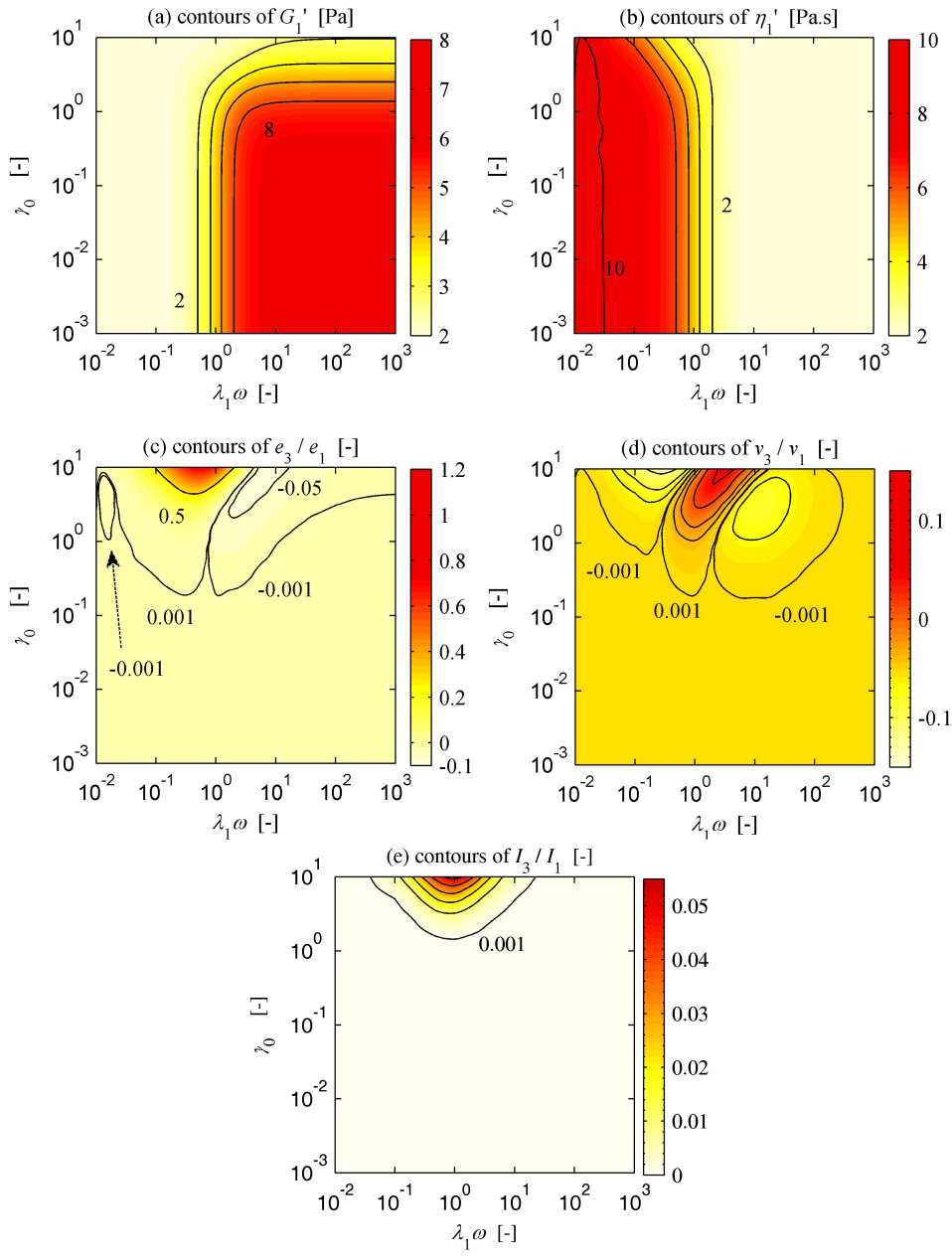
(a) contours of G_1' [Pa]
8
2
(b) contours of η_1' [Pa.s]
10
2
(c) contours of e_3 / e_1 [-]
0.5
-0.05
-0.001
0.001
-0.001
(d) contours of v_3 / v_1 [-]
-0.001
0.001
-0.001
(e) contours of I_3 / I_1 [-]
0.001
γ_0 [-]
$\lambda_1\omega$ [-]

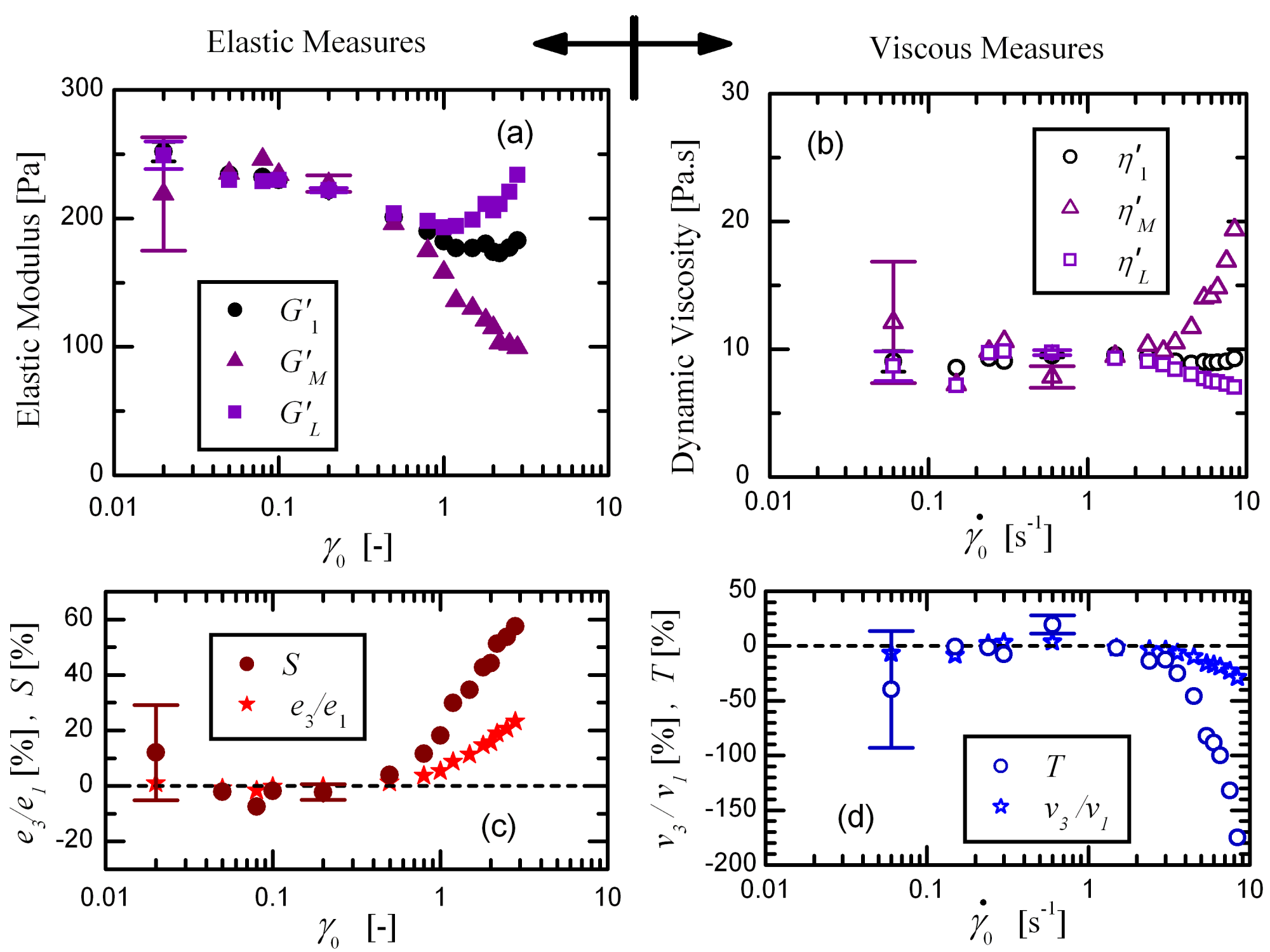
Elastic Measures
Viscous Measures
Elastic Modulus [Pa]
300
200
100
0
(a)
G'_1
G'_M
G'_L
0.01
0.1
1
10
γ_0 [-]
Dynamic Viscosity [Pa.s]
30
20
10
0
(b)
η'_1
η'_M
η'_L
$\dot{\gamma}_0$ [s^{-1}]
e_3/e_1 [%], S [%]
60
40
20
0
-20
S
e_3/e_1
(c)
v_3/v_1 [%], T [%]
50
0
-50
-100
-150
-200
T
v_3/v_1
(d)

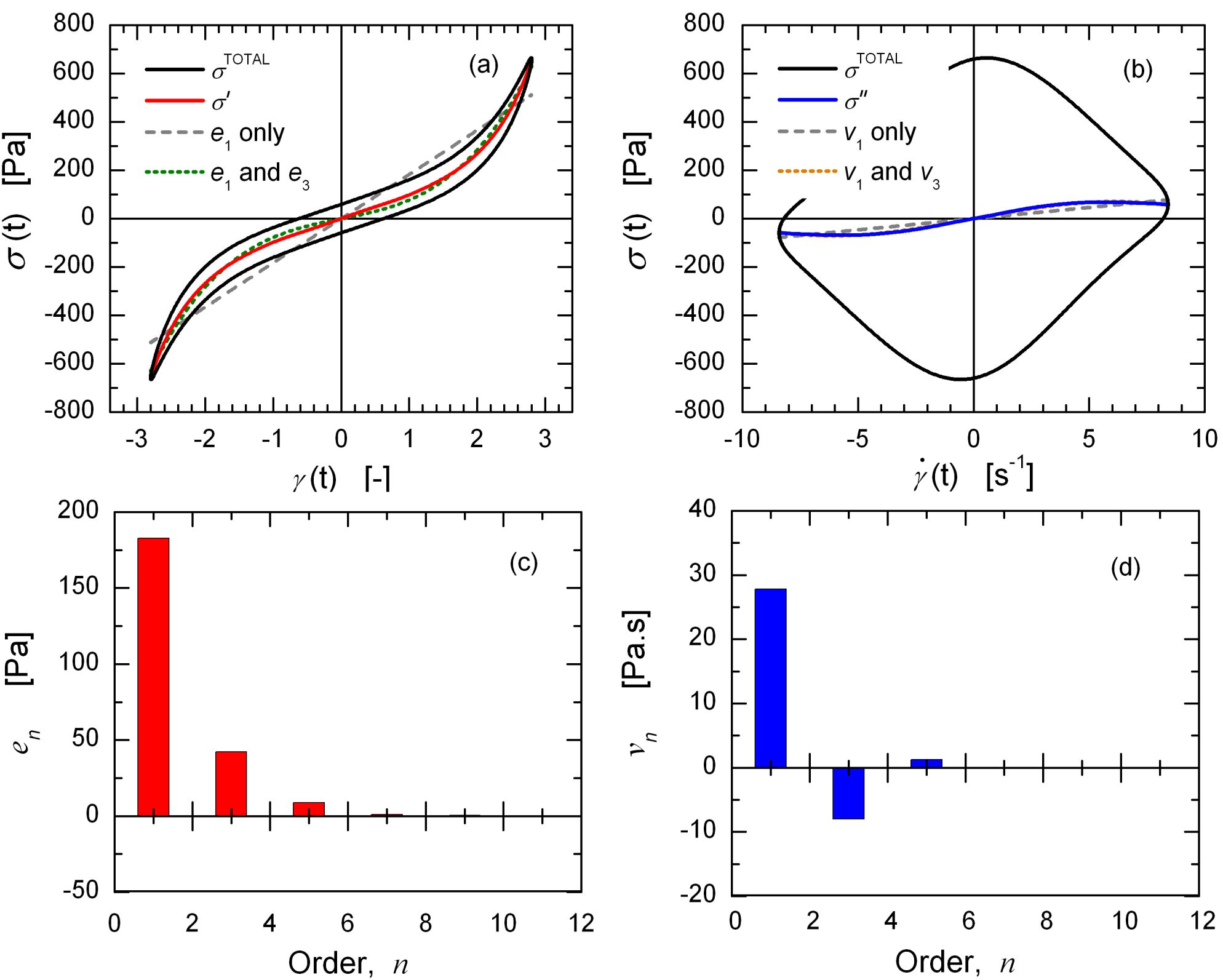
(a)
σ TOTAL
σ′
e1 only
e1 and e3
σ (t) [Pa]
γ (t) [-]
(b)
σ TOTAL
σ″
v1 only
v1 and v3
σ (t) [Pa]
γ̇ (t) [s-1]
(c)
en [Pa]
Order, n
(d)
νn [Pa.s]
Order, n

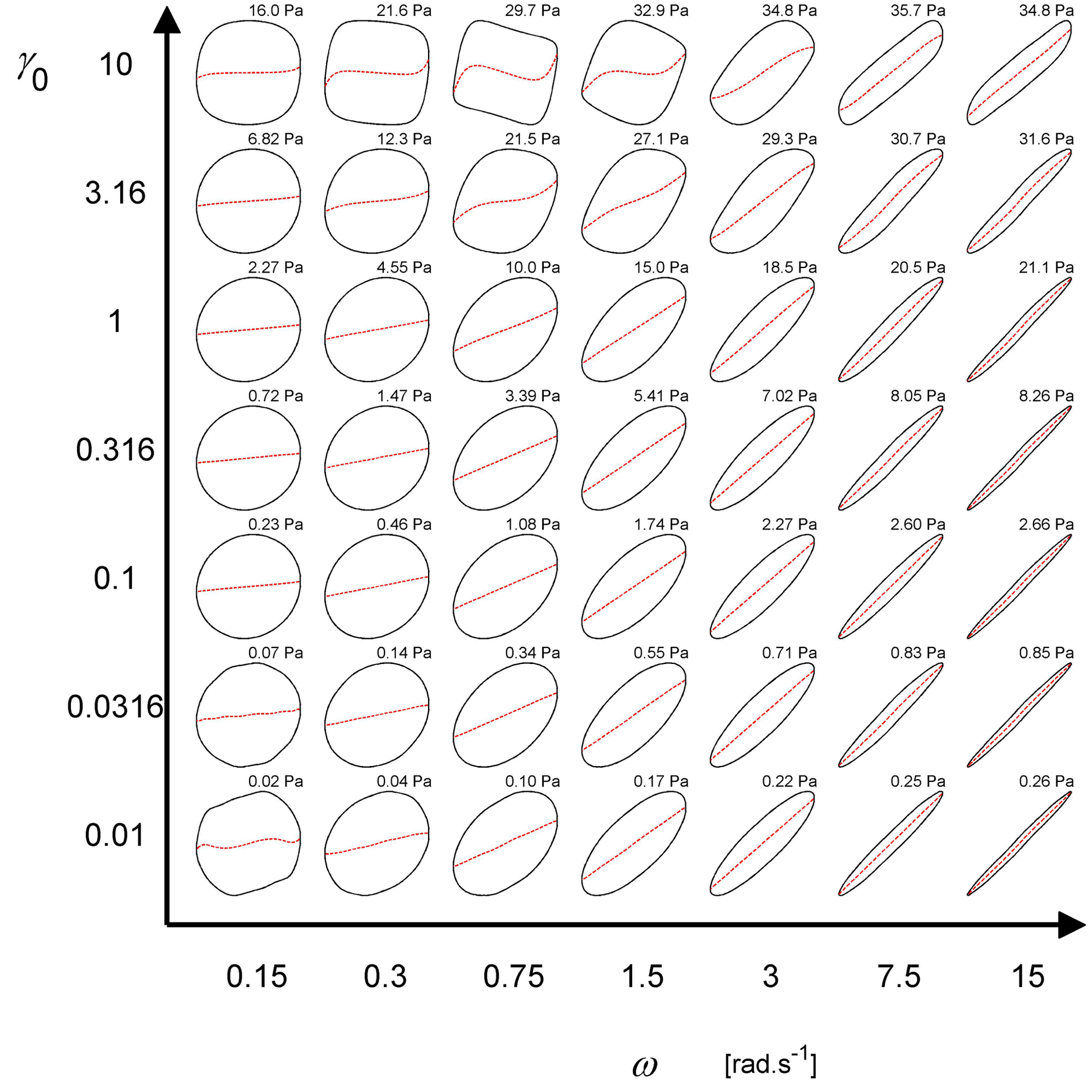
γ_0
10
3.16
1
0.316
0.1
0.0316
0.01
16.0 Pa
21.6 Pa
29.7 Pa
32.9 Pa
34.8 Pa
35.7 Pa
34.8 Pa
6.82 Pa
12.3 Pa
21.5 Pa
27.1 Pa
29.3 Pa
30.7 Pa
31.6 Pa
2.27 Pa
4.55 Pa
10.0 Pa
15.0 Pa
18.5 Pa
20.5 Pa
21.1 Pa
0.72 Pa
1.47 Pa
3.39 Pa
5.41 Pa
7.02 Pa
8.05 Pa
8.26 Pa
0.23 Pa
0.46 Pa
1.08 Pa
1.74 Pa
2.27 Pa
2.60 Pa
2.66 Pa
0.07 Pa
0.14 Pa
0.34 Pa
0.55 Pa
0.71 Pa
0.83 Pa
0.85 Pa
0.02 Pa
0.04 Pa
0.10 Pa
0.17 Pa
0.22 Pa
0.25 Pa
0.26 Pa
0.15
0.3
0.75
1.5
3
7.5
15
ω [rad.s^{-1}]

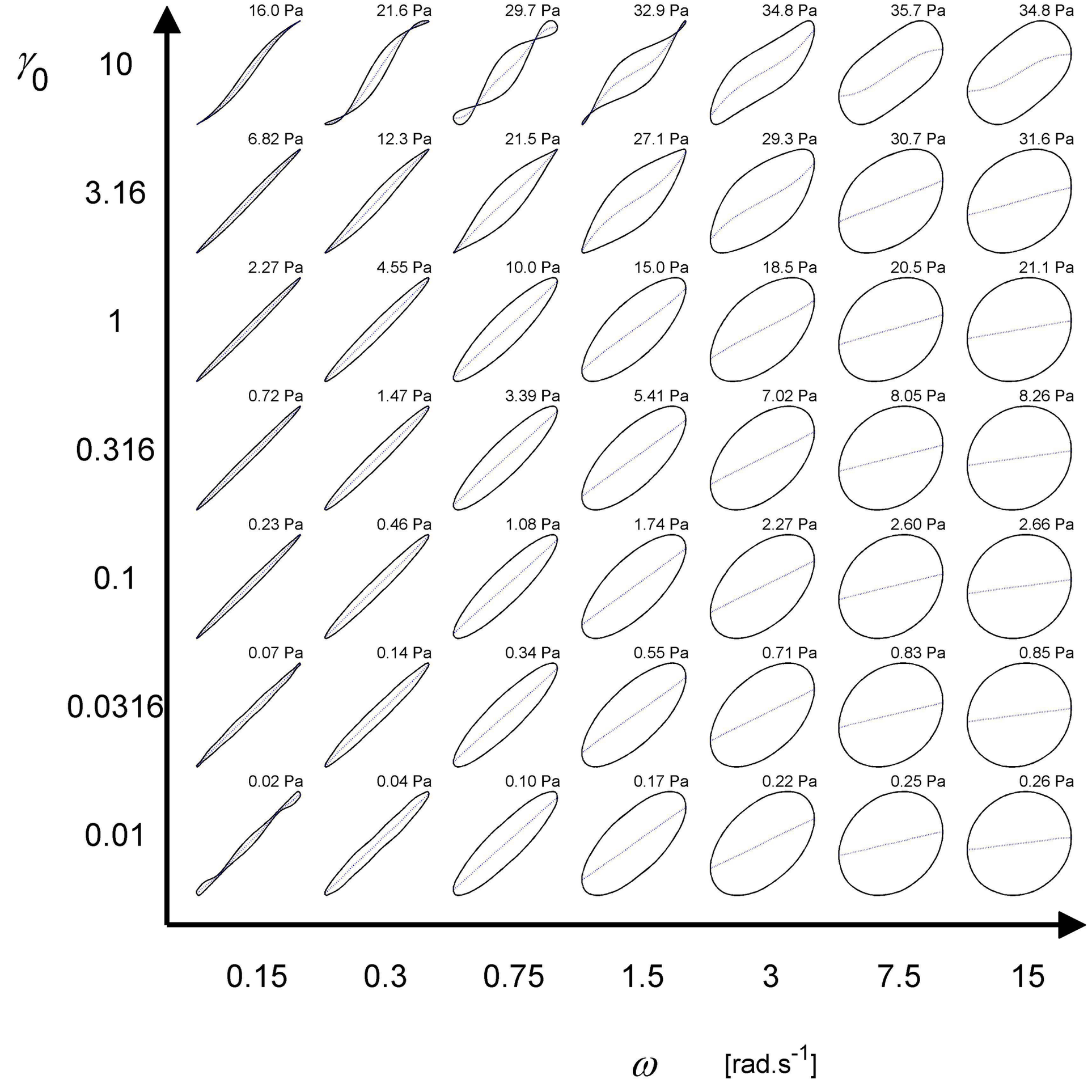
γ_0
10
3.16
1
0.316
0.1
0.0316
0.01
16.0 Pa
21.6 Pa
29.7 Pa
32.9 Pa
34.8 Pa
35.7 Pa
34.8 Pa
6.82 Pa
12.3 Pa
21.5 Pa
27.1 Pa
29.3 Pa
30.7 Pa
31.6 Pa
2.27 Pa
4.55 Pa
10.0 Pa
15.0 Pa
18.5 Pa
20.5 Pa
21.1 Pa
0.72 Pa
1.47 Pa
3.39 Pa
5.41 Pa
7.02 Pa
8.05 Pa
8.26 Pa
0.23 Pa
0.46 Pa
1.08 Pa
1.74 Pa
2.27 Pa
2.60 Pa
2.66 Pa
0.07 Pa
0.14 Pa
0.34 Pa
0.55 Pa
0.71 Pa
0.83 Pa
0.85 Pa
0.02 Pa
0.04 Pa
0.10 Pa
0.17 Pa
0.22 Pa
0.25 Pa
0.26 Pa
0.15
0.3
0.75
1.5
3
7.5
15
ω [rad.s^{-1}]

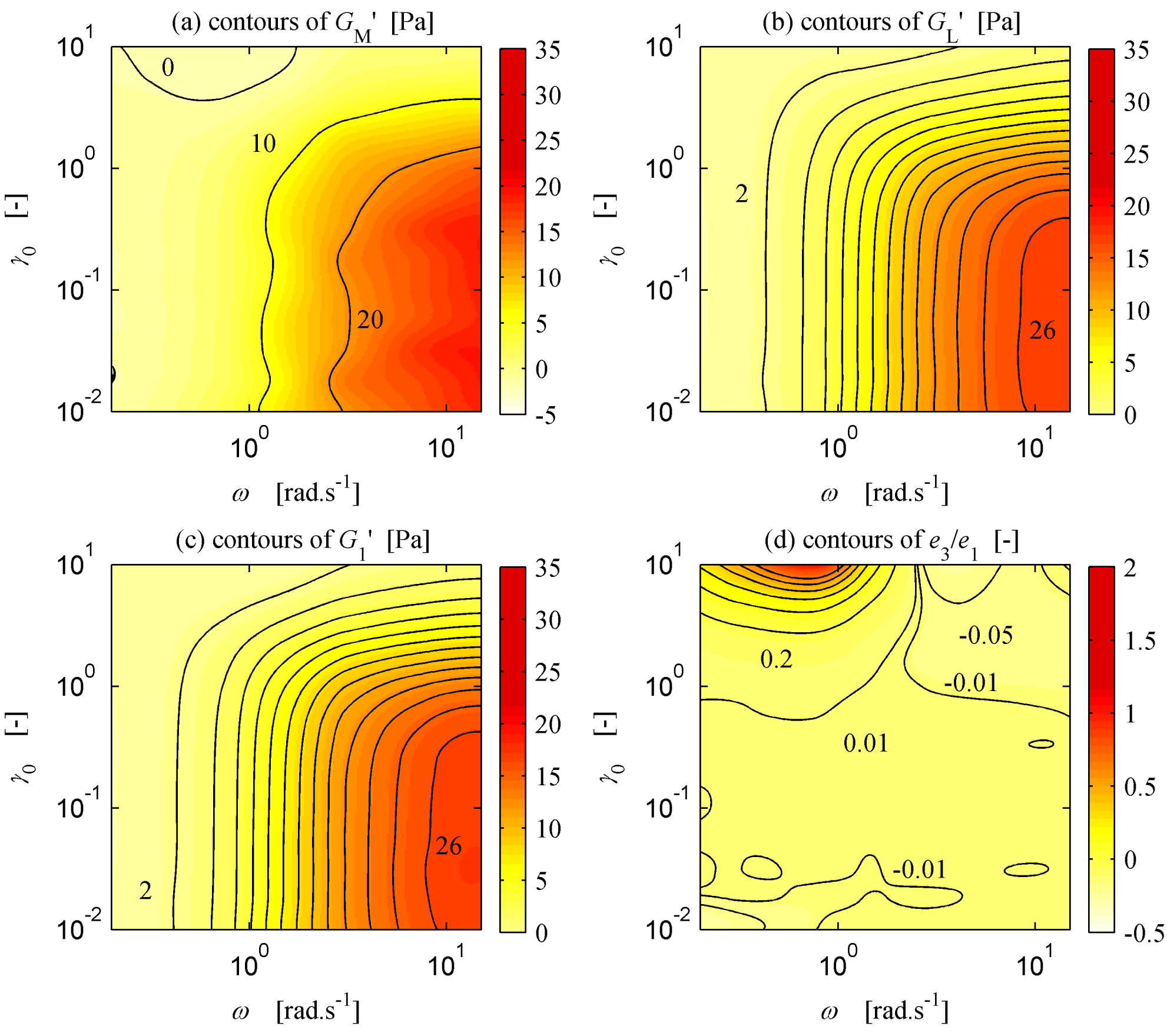
(a) contours of G_M' [Pa]
(b) contours of G_L' [Pa]
(c) contours of G_1' [Pa]
(d) contours of e_3/e_1 [-]
γ_0 [-]
ω [rad.s^{-1}]
0
10
20
2
26
0.2
-0.05
-0.01
0.01
-0.01

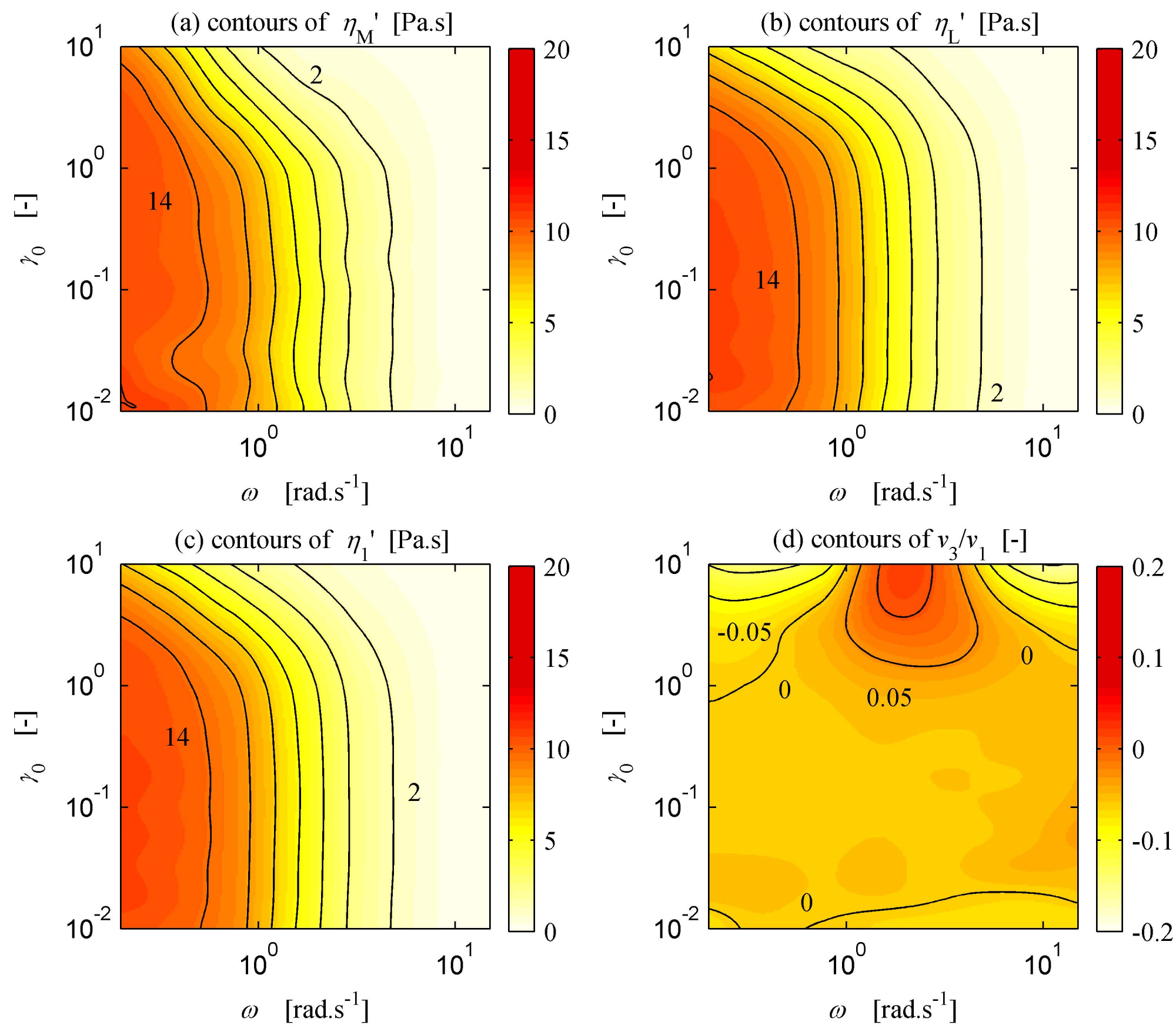
(a) contours of η_M' [Pa.s]
(b) contours of η_L' [Pa.s]
(c) contours of η_1' [Pa.s]
(d) contours of v_3/v_1 [-]
γ_0 [-]
ω [rad.s^{-1}]
10^{1}
10^{0}
10^{-1}
10^{-2}
2
14
-0.05
0
0.05
20
15
10
5
0
0.2
0.1
-0.1
-0.2

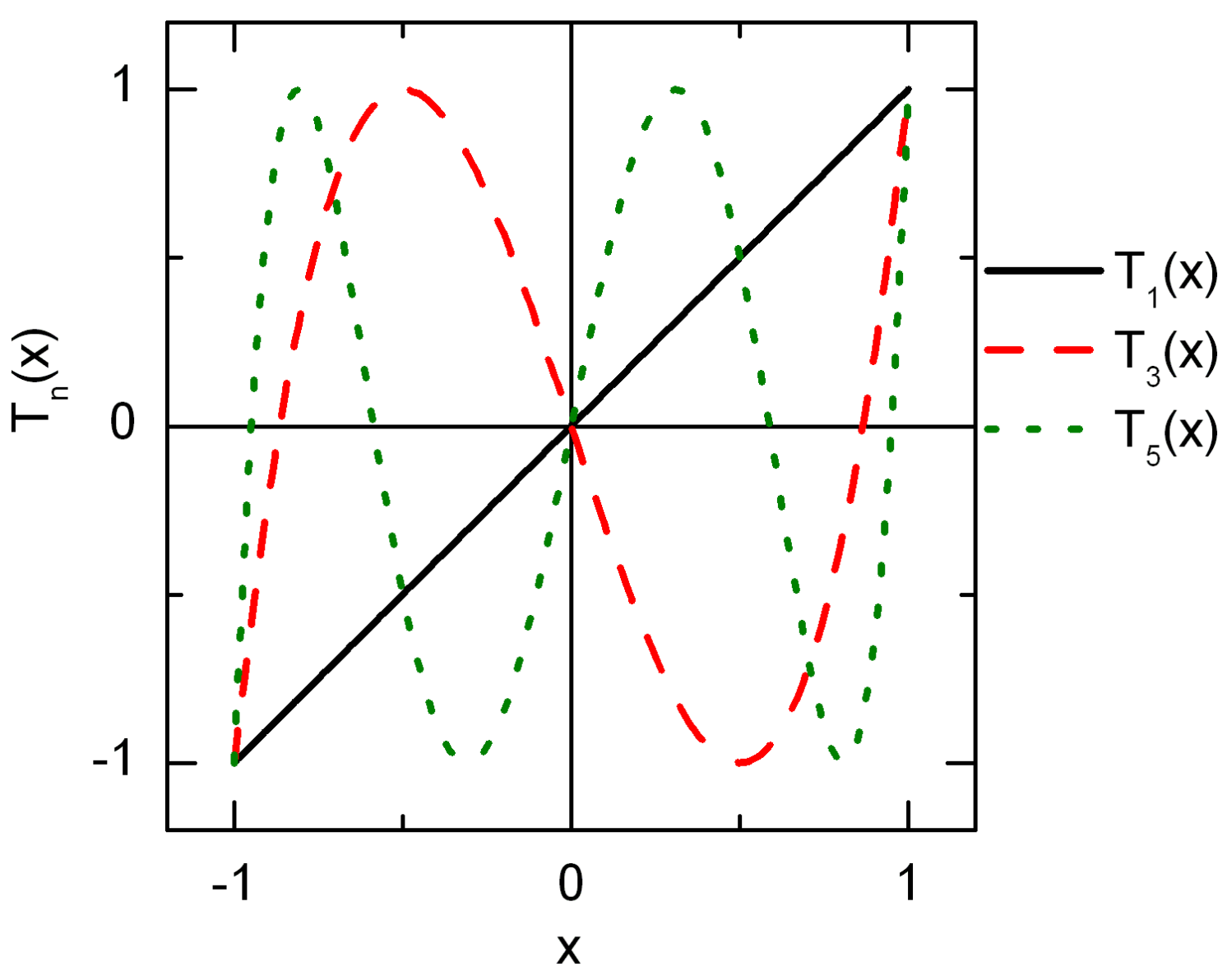
1
0
-1
-1
0
1
x
T_n(x)
T_1(x)
T_3(x)
T_5(x)

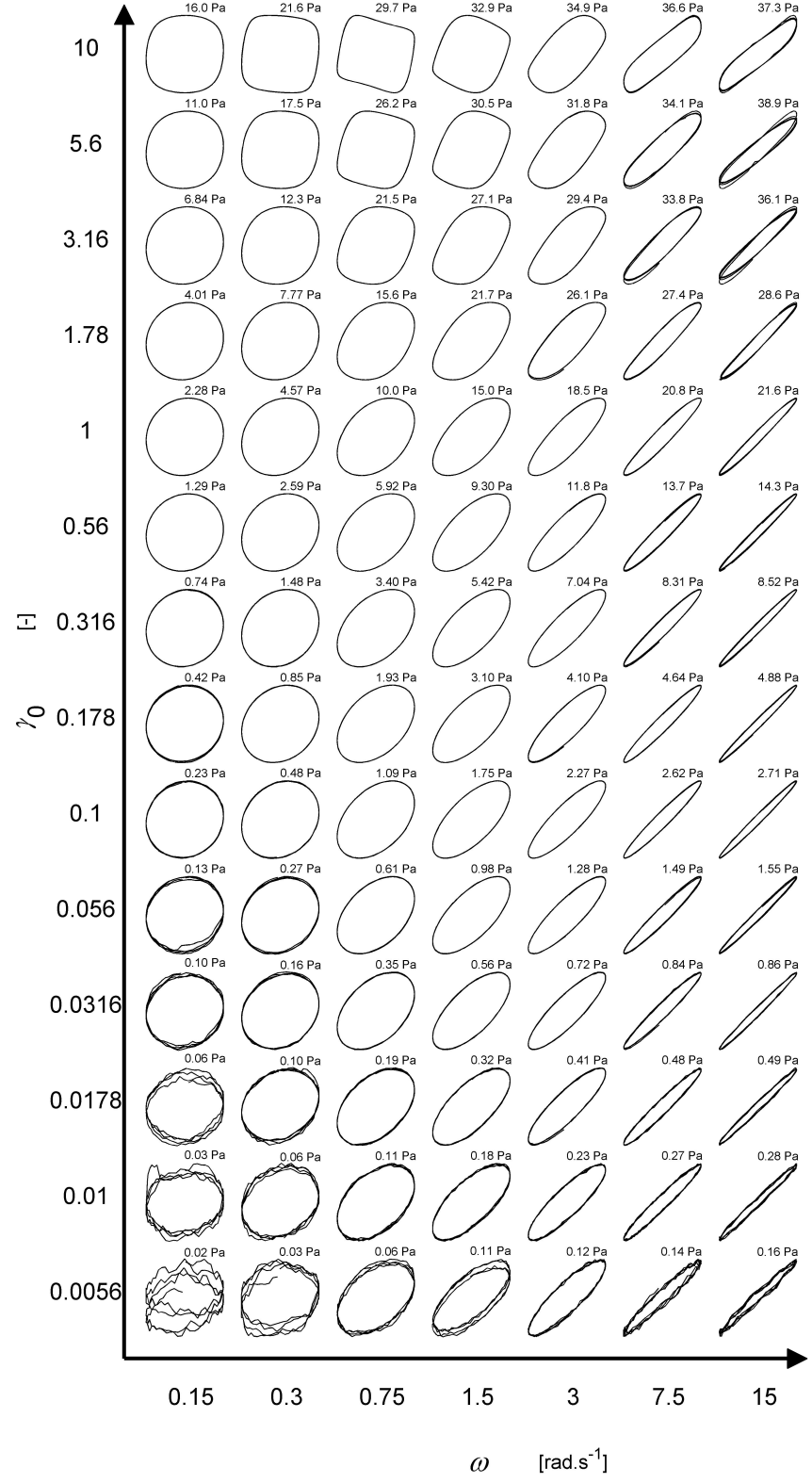
16.0 Pa
21.6 Pa
29.7 Pa
32.9 Pa
34.9 Pa
36.6 Pa
37.3 Pa
11.0 Pa
17.5 Pa
26.2 Pa
30.5 Pa
31.8 Pa
34.1 Pa
38.9 Pa
6.84 Pa
12.3 Pa
21.5 Pa
27.1 Pa
29.4 Pa
33.8 Pa
36.1 Pa
4.01 Pa
7.77 Pa
15.6 Pa
21.7 Pa
26.1 Pa
27.4 Pa
28.6 Pa
2.28 Pa
4.57 Pa
10.0 Pa
15.0 Pa
18.5 Pa
20.8 Pa
21.6 Pa
1.29 Pa
2.59 Pa
5.92 Pa
9.30 Pa
11.8 Pa
13.7 Pa
14.3 Pa
0.74 Pa
1.48 Pa
3.40 Pa
5.42 Pa
7.04 Pa
8.31 Pa
8.52 Pa
0.42 Pa
0.85 Pa
1.93 Pa
3.10 Pa
4.10 Pa
4.64 Pa
4.88 Pa
0.23 Pa
0.48 Pa
1.09 Pa
1.75 Pa
2.27 Pa
2.62 Pa
2.71 Pa
0.13 Pa
0.27 Pa
0.61 Pa
0.98 Pa
1.28 Pa
1.49 Pa
1.55 Pa
0.10 Pa
0.16 Pa
0.35 Pa
0.56 Pa
0.72 Pa
0.84 Pa
0.86 Pa
0.06 Pa
0.10 Pa
0.19 Pa
0.32 Pa
0.41 Pa
0.48 Pa
0.49 Pa
0.03 Pa
0.06 Pa
0.11 Pa
0.18 Pa
0.23 Pa
0.27 Pa
0.28 Pa
0.02 Pa
0.03 Pa
0.06 Pa
0.11 Pa
0.12 Pa
0.14 Pa
0.16 Pa
10
5.6
3.16
1.78
1
0.56
0.316
0.178
0.1
0.056
0.0316
0.0178
0.01
0.0056
γ_0 [-]
0.15
0.3
0.75
1.5
3
7.5
15
ω [rad.s^{-1}]